Article:
Steventon, MJ, Jackson, CA-L, Johnson, HD et al. (2020) Lateral variability of shelf edge and basin floor deposits, Santos Basin, offshore Brazil. Journal of Sedimentary Research, 90 (9). pp. 1198-1221. ISSN: 1527-1404

https://doi.org/10.2110/jsr.2020.14

Lateral variability of shelf edge and basin floor deposits, Santos Basin, offshore Brazil

Michael J. Steventon[1*], Christopher A-L. Jackson[1], David M. Hodgson[2] & Howard D. Johnson[1]

[1]Basins Research Group (BRG), Department of Earth Science & Engineering, Imperial College, Prince Consort Road, London, SW7 2BP, UK

[2]School of Earth and Environment, University of Leeds, Leeds, LS2 9JT, UK

Contact: michael.steventon13@imperial.ac.uk

Word count: 9468 (main body), 1053 (figure captions), 2966 (references)

ABSTRACT

Construction of continental margins is driven by sediment transported across the shelf to the shelf edge, where it is reworked by wave, tide, and fluvial processes within deltas and flanking clastic shorelines. Stalling of continental-margin progradation often results in degradation of the outer shelf to upper-slope, with sedimentation to the lower slope and basin floor via a range of sediment gravity flows and mass-movement processes. Typically, our understanding of how these processes contribute to the long-term development of continental margins has been limited to observations from broadly two-dimensional, subsurface and outcrop datasets. Consequently, the three-dimensional variability in process regime and margin evolution is poorly constrained and often underappreciated. We use a large (90 km by 30 km, parallel to depositional strike and dip, respectively) post-stack time-migrated 3D seismic-reflection dataset to investigate along-strike variations in shelf-margin progradation and outer shelf to upper-slope collapse in the Santos Basin, offshore SE Brazil. Early Paleogene to Eocene progradation of the shelf-margin is recorded by spectacularly imaged, SE-dipping clinoforms. Periodic failure of the outer shelf and upper-slope formed *c.*30 km wide (parallel to shelf-margin strike) slump scars, which resulted in a strongly scalloped upper-slope. Margin collapse caused (1) the emplacement of slope-attached mass-transport complexes (MTCs) (up to *ca.* 375 m thick, 12+ km long, 20 km wide) on the proximal

basin floor, and (2) accommodation creation on the outer shelf to upper-slope. This newly formed accommodation was infilled by shelf edge delta clinoforms (up to 685 m thick), that nucleated and prograded basinward from the margin-collapse headwall scarp, downlapping onto the underlying slump scar and/or MTCs. Trajectory analysis of the shelf edge deltas suggests that slope degradation-created accommodation was generated throughout the sea-level cycle, rather than during base-level fall as would be predicted by conventional sequence-stratigraphic models. Our results highlight the significant along-strike variability in depositional style, geometry, and evolution that can occur on this and other continental margins. Coeval strata, separated by only a few kilometres, display strikingly different stratigraphic architectures; this variability, which could be missed in 2D datasets, is not currently captured in conventional 2D sequence stratigraphic models.

Keywords: shelf edge deltas, mass-transport complexes/deposits (MTC/MTD), toe-of-slope fans/lobes, continental margins, sequence stratigraphy, clinoform, clinothem, trajectory analysis

INTRODUCTION

The shelf edge break is a dynamic area of erosion, deposition, degradation, and sediment bypass, forming the staging area for deep-water deposits. The principal accretionary unit of basin margins, the clinothem (bounded by clinoforms), records the interplay between shallow-marine and slope-related gravitational processes, and fluctuations in sediment supply, relative sea-level change, and accommodation. Since there are no accessible modern analogues, due to the Holocene transgression, our understanding of shelf edge/basin margin settings relies heavily on subsurface data, augmented by the development of sequence stratigraphic concepts (Mitchum et al. 1977; Vail et al. 1977; Weimer 1989; Van Wagoner et al. 1990; Hunt and Tucker 1992; Posamentier et al. 1992; Catuneanu 2006; Neal et al. 2016). These concepts have been extended further through shelf edge (shoreline) trajectory analysis, which considers the influence of sediment supply and relative sea-level changes on the stratigraphic architecture and facies distributions along shelf edges (Helland-Hansen and Gjelberg 1994; Helland-Hansen and Martinsen 1996; Steel and Olsen 2002; Carvajal et al. 2009; Helland-Hansen and Hampson 2009). However, the role of outer shelf to upper-slope degradation and along-strike depositional variability on shelf edge development, and their coupled impact on sequence-stratigraphic models, has received less attention (e.g. Neal and Abreu 2009). This partly reflects the fact that deposits and shelf edge trajectories associated with degradational phases are poorly preserved, and because most studies are largely two-dimensional (2-D). There have been recent reassessments of concepts such as along-strike variability (Madof et al. 2016) and three-dimensionality (Burgess 2016) in shelf edge process and product (Deibert et al. 2003; Dixon et al. 2012; Cosgrove et al. 2018), and the general non-uniqueness of stratigraphic patterns when trying to determine autogenic versus allogenic controls (Muto et al. 2007; Burgess and Prince 2015; Hampson 2016; Zhang et al. 2019). In this context, there is a case for revaluating basin margins characterized by major degradational phases, and along-strike variability in depositional system type and stratigraphic architecture (Fig.1).

Shelf edge areas with degradational phases form through a combination of pre-conditioning factors (e.g. slope oversteepening, relative sea-level change, mobile substrates, etc.), which cause upper-slope gradients to exceed a stable equilibrium (e.g. Ross et al. 1994; Adams and Schlager 2000; Locat and Lee 2002; Sultan et al. 2004; Prather et al. 2017). These out-of-grade systems can achieve grade by the outer shelf to upper-slope failing, resulting in the downdip deposition of

mass-transport complexes/deposits (MTCs) and the formation of canyon- or channel-like sediment conduits (Galloway 1998). Degradation-influenced sequences are generally characterized by a repetitive cycles of (i) shelf edge to upper-slope failure and the formation of scarps (60 km in width, up to 825 m in height), (ii) deposition of toe-of-slope MTCs that may onlap landward against previously deposited slope deposits, (iii) further mass wasting and sediment bypass, and (iv) infilling or "healing" of the evacuated area by shelf edge deposits (e.g. Gomis-Cartesio et al. 2018; Proust et al. 2018). Although there are exceptions (e.g. McMurray and Gawthorpe 2000; Jones et al. 2015), most stratigraphic models that document some form of shelf edge failure are based on predominantly 2-D datasets, most typically from outcrop (e.g. Dixon et al. 2013; Peng et al. 2017; Gomis-Cartesio et al. 2018) and therefore only capture a snapshot of the system architecture, and not the full along-strike variability.

The principal aims of this study are to (i) characterize a shelf edge system during multiple periods of progradation and degradation, and (ii) determine the geological controls on the lateral variability of the Paleocene-Eocene outer shelf to slope depositional system in the Santos Basin, offshore Brazil (Fig. 2). This is achieved through a detailed seismic facies analysis of a 3D seismic-reflection dataset, which provides continuous high-quality imaging of an area extending for *ca.* 90 km along depositional strike and *ca.* 30 km along depositional dip. The main objectives are to: (i) describe the distribution of depositional elements along the full along-strike length of the margin during multiple phases of construction and degradation, (ii) use clinoform trajectory analysis to characterize sediment partitioning relationships between the shelf edge and basin floor, (iii) evaluate the potential driving mechanisms for periodic shelf edge collapse, and (iv) develop a predictive, three-dimensional stratigraphic model for margins with constructional and degradational phases.

BASIN SETTING

The Santos Basin is located in the Central Segment of the South Atlantic (Fig. 2), bounded to the north east by the Cabo Frio High and to the south by the Florianópolis Fracture Zone (Meisling et al. 2001; Torsvik et al. 2009). The basin formed in response to the Gondwanan break-up cycle, which propagated from the south, reaching the Florianópolis Fracture Zone during the Early Cretaceous (e.g. Clemson et al. 1997; Meisling et al. 2001; Karner and Gambôa 2007; Mohriak et al. 2008). The tectono-stratigraphic evolution of the basin is defined by four megasequences (Fig. 3): (i) a syn-rift phase (Hauterivian to Aptian), (ii) a transitional "sag" phase (Aptian) (i.e. earliest post-rift), during which time a thick (c.2.5 km; Davison et al. (2012)) evaporite-dominated sequence was deposited, (iii) a restricted marine phase (Albian) (i.e. early post-rift), and (iv) a fully marine, passive margin phase (Cenomanian to present) (i.e. main post-rift phase) (Chang et al. 1992; Meisling et al. 2001; Guerra and Underhill 2012). This study focuses on the Paleogene period of the passive margin phase (Fig. 3).

From the Late Cretaceous to Early Paleogene, a thick clastic wedge prograded south eastwards into the Santos Basin (Figs. 3 & 4) (Macedo 1989; Guerra and Underhill 2012). This sediment flux was driven by periodic regional uplift of the onshore Serra do Mar and Serra da Mantiqueira coastal ranges (Cobbold et al. 2001; Saenz et al. 2003), which exceeded a global eustatic sea-level high, allowing sand-rich systems to prograde beyond the previous drowned Albian carbonate shelf (Modica and Brush 2004). Onshore tectonic readjustment in the latest Cretaceous to Early Paleocene, reorganized the drainage networks to have a NE trend (ancestral Paraiba do Sul river system), shifting the loci of sedimentation northwards towards the central and northern Santos Basins (Cobbold et al. 2001; Modica and Brush 2004; Duarte and Viana 2007). Shelf edge deltas developed during the Paleocene in the central and northern Santos Basin (Fig. 2), while areas to the south were sediment starved (Modica and Brush 2004). The Eocene records continued progradation of shelf edge deltas and forms the focus of this study. The succession is dissected by a middle Eocene (40-43 Ma) erosion surface that formed due to large-scale collapse of the margin. This event remobilised material on the delta topsets and foresets, resulting in the deposition of MTCs and turbidites that form hydrocarbon-bearing reservoirs in the north of the basin (Fig. 2; Atlanta and Oliva fields) (Ebiwonjumi and Schwartz 2003). The Eocene shelf edge deltas are capped by a regionally extensive Early Oligocene flooding surface (Fig. 3). This regionally mappable surface (see below) records a global marine highstand, which drove landward-directed backstepping of the shelf edge break by >35 km (Fig. 3).

From the late Paleogene to the present-day, deposition in the central Santos Basin has been dominated by a contourite drift system (Duarte and Viana 2007). During this time, tectonic reorganisation of the onshore terranes resulted in diversion of the ancestral Pariba do Sul river into the Campos Basin (Karner and Driscoll 1999). This is manifested in synchronous retrogradation and progradation of shorelines in the northern Santos (which was sediment starved) and Campos Basin (which was sediment nourished, being now fed by the Pariba do Sul river), respectively. In the southern and central Santos Basin, a new sediment source initiated during the Neogene, recorded by thick sediment packages (e.g. Williams and Hubbard 1984), renewed progradation, and widespread mass-wasting (Figs. 3 & 4).

DATASET AND METHODS

Dataset

This study utilises a c. 3600 km^2, post-stack time-migrated (PSTM) 3D seismic-reflection survey located in the Southern Embayment of the Santos Basin, offshore Brazil. The data straddle the modern day shelf edge break between the São Paulo and Merluza transfer zones (SPTZ and MTZ) (Modica and Brush 2004) (Fig. 2). The data are SEG normal polarity (American polarity, i.e. an increase in acoustic impedance = peak), zero-phased, and have a processing bin spacing of 25 m by 12.5 m. Vertical resolution (VR) within the Paleocene-Eocene interval of interest is c. 28 m, assuming a velocity of 2750 ms^{-1} estimated from Berton and Vesely (2016) and a dominant frequency of 24 Hz (extracted directly from the seismic data).

Seismic Interpretation

The survey images the first four seconds two-way time (TWT) of post-salt succession (*c.* 5.5 km thick), including the main Paleocene-Eocene progradational phase. No wells were available, with ages and velocities estimated through calibration with regional studies (Modica and Brush 2004; Davison 2007; Berton and Vesely 2016). We map two basinwide flooding surfaces in this succession, approximately Maastrichtian-Paleocene (*ca.* 55-59 Ma) and Early Oligocene (*ca.* 30-

35 Ma) in age. Locally, we map an Eocene (*ca.* 40-43 Ma) erosion surface that is restricted to the outer shelf to upper-slope of one of the clinothems developed within the Paleocene-Eocene progradational succession. We mapped top Aptian salt to determine potential structural (and related subsidence) controls on the style of margin progradation (see supplementary material). We used the following geometric-, amplitude- and frequency-based attributes to image the various depositional systems of interest: (i) variance (coherency) (see Van Bemmel and Pepper 2000), (ii) root-mean-squared (RMS) amplitude, and (iii) spectral decomposition (see Partyka et al. 1999) (frequency spectra can be found in the supplementary material).

Shelf edge Trajectory Analysis

Shelf edge trajectories define the spatial and temporal migration of clinoform rollover points during aggradation, progradation, and retrogradation, and can be used to divide sedimentary units into discrete genetic packages (see Helland-Hansen and Martinsen 1996). Shelf edge trajectories reflect the interplay between sediment supply and accommodation (see Helland-Hansen and Hampson 2009), and can aid prediction of sand supply to basin margins and reservoir presence in deep-water settings (e.g. Steel and Olsen 2002). The basin margin setting in our study area is characterized by large clinoforms (*ca.* 275-685 m thick) that comprise well-defined topsets (shelf), foresets (slope), and bottomsets (basin floor). Clinoform rollover points separate low-angle (<1°) topsets from high-angle (up to 6°) foresets.

Shelf edge trajectories are often grouped into three main categories: (i) rising-/ascending-seaward trajectories, reflecting highstand and/or normal regression, (ii) rising-/ascending-landward trajectories, reflecting coastal retrogradation (transgression), and (iii) falling-/flat trajectories, reflecting lowstand and/or forced regressive conditions (Posamentier et al. 1992; Helland-Hansen and Martinsen 1996; Helland-Hansen and Hampson 2009). Rising trajectories of both regressive and transgressive types can promote sediment storage on the shelf, whereas falling trajectories may (but need not always; e.g. Burgess and Hovius 1998; Carvajal and Steel 2006; Cosgrove et al. 2018) be related to shelf incision, river-mouth sediment bypassing, and delivery of sand-grade material to deep-water settings (e.g. Johannessen and Steel 2005).

In this study, the trajectory of the Paleogene-Eocene shelf edge is obtained by plotting clinoform rollover points from six dip-oriented sections that are datumed on the Early Oligocene flooding surface (green horizon), where it is located in a topset position. This surface was chosen as the datum because it is laterally extensive across the Eocene and Paleocene deltas and has only a minor basinward dip (<1° on the shelf directly above the clinoform rollover points) (Fig. 4). The clinoform rollover points (shelf edge) are defined by geometrically linking two tangent lines from the topsets and foresets, finding the intersection, and then tracing orthogonally from these points.

Volumetric-Based Sediment Flux (Q)

Time-structure maps (Maastrichtian-Paleocene and Early Oligocene) were depth converted using estimated sediment velocities (*c.* 2750 ms^{-1}) (Berton and Vesely 2016). The resulting depth-structure maps where then decompacted to remove the effects of burial-related porosity reduction and hence provide an estimate of the pre-compaction thickness of the Maastrichtian-Paleocene to Early Oligocene time-interval (T_a). The time-interval represented by these units is based on estimates of the ages of the bounding surfaces, which are themselves are estimated from data presented by Modica and Brush (2004). The decompacted volume was used to estimate the gross sediment flux (Q) for the study area, along with the change along strike of the shelf edge from north to south. The resulting values of sediment flux are minimum estimates, given the incomplete imaging of the complete depositional system (i.e. distal basin floor and uppermost coastal plain). Specifics of the calculations are detailed in the supplementary material, with the first-order sediment flux estimated by

$$Q = \frac{V_c \times D}{T_a} \qquad (1)$$

where V_c = compacted volume, D = compaction correction (see Supplementary material).

SEISMIC FACIES ANALYSIS

This analysis focuses on the Paleocene-Eocene progradational systems, particularly the along-strike variability of the shelf-slope-basin floor succession and the repetitive nature of shelf edge failure. The interval is bound by two, regionally extensive marine flooding surfaces: (1) the Maastrichtian-Paleocene, and (2) the Early Oligocene (Figs 3 & 5). This interval comprises two major progradational sequences, separated by a composite middle Eocene erosion surface (Fig. 4). The thickness of the Paleocene to Early Oligocene sedimentary wedge ranges from 700 ms (*ca.* 965 m) in the north to <300 ms (*ca.* 415 m) in the south (Fig. 5ii). The terminology used in the following section is based on clinoform dip angles: shelf (<1°), slope (<6°), and basin floor (sub-horizontal), which are contained within the larger, continental margin-scale system (see Patruno et al. 2015). The terms shelf edge and mid-shelf deltas (see Porębski and Steel 2003) are here synonymous with shelf edge and delta-scale/shoreline clinoforms (e.g. Patruno and Helland-Hansen 2018), respectively. An overview of the seismic facies, which essentially form the "building blocks" of the (seismically imaged) margin, are outlined in Table 1. An index map has been included to navigate between figure locations (see Fig. 5). The boundaries of the northern, central and southern areas of the dataset can be found in Figure 2. We describe twelve seismic facies in order of location along a clinothem, from shelf to basin floor. Their amplitude and geometrical characteristics and interpreted depositional environments can be found in Tables 1 and 2.

Shelf

SF1: Landward-diverging, low- to high-amplitude, continuous reflections (shelf).---

Description: SF1 is composed of parallel to landward diverging, sub-horizontal, and highly continuous reflections (Fig. 6). The packages are dominantly low-amplitude, and are capped by high-amplitude continuous reflections, which we interpret as flooding surfaces (i.e. Maastrichtian-Paleocene and Early Oligocene). At the shelf edge, reflections are truncated by basinward-dipping erosion surfaces. In their landward part, sub-horizontal reflections are either incised by low- (SF2)

or high-amplitude (SF3) reflection packages, or merge with high-amplitude continuous packages (SF4) (Figs. 6, 7).

Interpretation: SF1 dominates the shelf and are accordingly interpreted to represent a shallow-marine shelf environment. Variations in acoustic impedance represent variable interbedding of sandstone-mudstone units, and/or variations in the cementation state of an otherwise, relatively (lithologically) homogenous sequence.

SF2: Incised low-amplitude surfaces and low-amplitude fill (incised valley and fill) .---

Description: SF2 comprises a low-amplitude composite erosion surface that extends along-strike for up to 17.5 km and downslope for 14 km on the northern shelf. This surface consists of a series of smaller (2.0-6.5 km wide), NW-trending erosional surfaces (Fig. 7) that decrease in amplitude and relief (100 ms to below vertical resolution) toward the shelf edge. Individual incision surfaces are filled by up to 100 ms (ca. 140 m) thick packages of predominantly low-amplitude, low frequency, moderate continuity reflections that onlap the basal erosion surface.

Interpretation: The scale, topset location, and relative position of SF2 to the shelf edge supports an interpretation of shelf-hosted incised valley-fills. Formation of these features may reflect prolonged periods of subaerial exposure, cannibalisation of the shelf, and sediment bypass to and beyond the shelf edge. The overlying deposits likely represent background shelf and/or estuarine mudstones, deposited during subsequent sea-level rise.

SF3: High-amplitude packages (fluvial channels).---

Description: SF3 is represented by 50-1350 m wide belts of erosionally based, sinuous packages of high-amplitude reflections (Fig. 7). Like SF2, these features are restricted to the northern and central areas (Fig. 7). SF3 is concentrated along the flanks and at the base of the larger incisional events (SF2). Individual high-amplitude events are no more than two seismic cycles thick, thinning to one cycle towards the shelf edge (c. 30 ms to vertical resolution).

Interpretation: The topset location of SF3, combined with its high-amplitude and sinuous planform support an interpretation of fluvial channel-fills genetically-related to the larger incised valley-fills

(SF2). Figure 7iv suggests that the sediment supply for the fluvial system may have been locally sourced from a salt-related high in the central to northern area of the shelf. More specifically, SF2/3 trends parallel to the shelf, suggesting sediment transport orthogonal to the dominant NW-SE trend of the nearby shelf edge.

SF4: Linear high-low amplitudes (beach ridges/strandplain) .---

Description: SF4 comprises a series of discrete, alternating high- and low-amplitude features (Fig. 8). They have an irregular relief, with the high-amplitude anomalies generally forming mounded features (c. 20 ms TWT/ca. 28 m high) that are separated by low-amplitude depressions or horizontal reflections. In plan-view, these high-/low-amplitude pairs form NW-trending, linear ridges and troughs that are 0.1-1 km wide and at least 28 km long (Fig. 8). Amplitude extractions show that the ridges are parallel to subparallel to one another, are spaced 0.15-2.0 km, and occur in sets that are separated by subtle angular discordances (Fig. 8iii). A composite seismic line through a single high-amplitude ridge demonstrates the remarkable continuity of these features (Fig. 8ii), showing that they migrate basinwards through time towards high-amplitude, continuous reflections (SF5). Within the same stratigraphic level as the linear features, a series low-amplitude, moderate to low frequency reflections are present. These are crescentic in map view, are up to 2.5 km long and 0.7 km wide and have the same NE-SW trend as the linear features (Fig. 8iii/iv).

Interpretation: The SF4 ridges are oblique to the survey geometry, are irregularly spaced, occur in clearly defined sets of subtly different trend, and show distinct amplitude patterns; this suggests that these features are geological, rather than a seismic acquisition artefact/footprint (e.g. Marfurt et al. 1998) (Fig. 8). Therefore, we interpret the low-amplitude, convex-up features as sandstone-dominated beach ridges within a strandplain environment (see Otvos 2000; Jackson et al. 2010). The occurrence of beach ridges suggests a wave-dominated shelf, fed by along-shore transported sediment. We interpret the spatially related crescent-shaped features as back-barrier lagoons/bays; these have similar plan-form geometries to features observed in off-axis positions of the modern Pariba do Sul delta system (Fig. 8v).

SF5: Isolated high-amplitude continuous reflections (foreshore/upper shoreface) .---

Description: SF2, 3 and 4 are overlain by a set of high-amplitude, continuous, high-to-moderate frequency reflections that are restricted to the mid-shelf areas and are capped by the early Oligocene flooding surface (Fig. 6i). They display the same NE-SW trend as SF4, occurring in elongate belts (c. 28 km). They are, however, wider (up to 6 km) and thicker (up to c. 75 m), tapering towards the NE. SF5 passes into low-amplitude/frequency, discontinuous seismic facies on the inner shelf.

Interpretation: SF5 shows many of the same characteristics as SF4 (i.e. the same NW-SW trending linear forms) suggesting a continuation of clastic shelf progradation. We therefore interpret SF5 to represent a foreshore to upper shoreface environment, with the high-amplitude bands potentially representing wide, sandstone-rich belts.

SF6: Parallel-oblique clinoforms (mid-shelf deltas) .---

Description: SF6 is composed of a series of parallel-oblique clinoforms (with some internal shingled and sigmoidal clinoforms) that downlap onto the shelfal deposits (SF1), and toplap or converge with semi-continuous, low-amplitude upper surfaces (Fig. 6). The clinoform foresets are 25-125 ms tall, up to 4250 m long, and up to 7.8 km along-strike width, and thin from up to 350 ms (*c.* 480 m) in the northern area to 175 ms (*c.* 240) in the southern area. The clinoform downlap terminations trend c. 058-238° in the northern area, shifting slightly to c. 042-222° farther south. Clinoforms document >19 km of progradation, pinching-out just before the shelf edge break (Fig.6). Internally the clinoforms have low-amplitude, low frequency, discontinuous to semi-continuous foresets that dip c. 2-3°, with topset convergence, and minor bottomset deposition/preservation. Clinoform trajectories are broadly flat. Above this prominent progradational succession are several additional, lower amplitude, progradationally to retrogradationally stacked, parallel-oblique clinoform-bearing sequences, with contourite drift deposits (e.g. Rebesco et al. 2014) dominating the upper-slope to basin floor (Fig. 4i).

Interpretation: We interpret SF6 to represent progradation of a mid-shelf delta in water depths of up to 75 ms (*c.* 100 m), and re-establishment of the shelf after early Oligocene flooding. The variation in clinoform downlap orientation in the central part of the shelf is likely due to syn-

depositional seabed deformation above a salt diapir (Fig. 6ii/iii). Overall, the shelf sequence suggests a primarily wave-dominated, strike-fed deltaic system, with minor fluvial input.

Outer shelf to Upper-Slope

Mid-Eocene scarp.---

The outer shelf to upper-slope is dominated by progradational-to-aggradational clinoform sets and related failure scarps, which vary in frequency and size along-strike. However, one main "composite" scarp is pervasive throughout the Paleocene-Eocene succession, cross-cutting multiple levels of stratigraphy, ranging in height from 600 ms (*c.* 825 m) in the NW to 50 ms (*c.* 69 m) in the SE, and pinching out toward the south of the study area (Fig. 5iv & 10i). The scarp is arcuate in planform and trends broadly NE-SW, dipping at ~6-7° and extending along-strike for 60 km. In section, the scarp is either linear (i.e. in the northern part of the study area; Fig. 9i, 12i) or highly irregular and scalloped (i.e. in the central part of the study area; Fig 9ii). Modica and Brush (2004) identified this regional middle Eocene scarp, showing that it extends along-strike for >250 km. Our work shows that this interpretation can be extended south of the São Paulo transfer zone for another 50 km, terminating in the south of our study area.

SF7: Small-sigmoidal clinoforms (proto-shelf edge deltas).---

Description: SF7 consists of low-relief (typically 75-150 ms/*ca.* 105-205 m thick), low-angle (1-3°) clinothems (Fig. 9). Cross-sectional geometries vary between sigmoidal to oblique-sigmoidal, with clinoforms downlapping underlying erosion surfaces (Fig. 9ii). The foresets are defined by low-amplitude, semi-continuous to discontinuous reflections. The clinoform heights periodically increase basinward, from <50ms to >150ms, before passing downdip into SF8 (see below). Clinoform topsets display both low and high amplitudes. Bottomsets vary along-strike, being characterized by either; (i) low-amplitude, discontinuous reflections; (ii) high-amplitude, isolated (c. <1 km along-strike), single-cycle reflections that are concentrated near the composite scarp; or (iii) thicker (c. 75 ms or 105 m), high-amplitude, chaotic reflections that, in many cases, are bound

downdip by a terminal ramp (Fig. 9ii). Where preserved, SF7 clinoform-bearing sequences display falling to flat trajectories.

Interpretation: Locally, SF7 is developed along up to 5 km strike-length of the shelf edge to upper-slope, typically being ponded in the middle Eocene scarp. We interpret SF7 to represent the initial nucleation and progradation of shelf edge deltas after formation of the irregular upper-slope scarp, an interpretation supported by its position on the upper-slope and the fact its caps the middle Eocene scarp. Progradation of these deltas healed relief associated with the precursor shelf edge/upper-slope failure.

SF8 and 9: Large-sigmoidal clinoforms (shelf edge deltas).---

Description: SF8 and 9 are dominated by clinoforms that are larger (*ca.* 200-500 ms or ca. 275-685 m tall) and steeper (ca. 5-6° dips) than those characterized by SF7. Clinoforms are sigmoidal to oblique-sigmoidal, extending along-strike for up to 20 km (Fig. 9i/ii). Amplitudes vary across the clinoform foresets. In central and southern areas, foresets are defined by continuous low- to moderate-amplitude reflections, whereas the bottomsets are low- to moderate-amplitude reflections of limited lateral continuity, whereas in the northern areas, foresets are seismically similar, but bottomsets have higher amplitudes and extend for up to 5 km along-strike (Fig. 9). The foresets in the central and northern area also contain isolated high-amplitude chaotic packages (SF9) that are c. 180-1650 m long, 75-200 m wide, and 25-50 ms (*c.* 35-70 m) thick. These packages trend parallel to clinoform dip and are concentrated directly downdip of SF7 or within the foresets of SF8. Many of the clinoform sets display offlap geometries and topset truncation, resulting in limited topset preservation. We observed a consistent stacking pattern, with SF9 at the base of a sequence, where reflection continuity is poorer, moving stratigraphically upward into SF8, where foresets and bottomset reflections become more continuous and dips decrease.

Interpretation: After initial nucleation of clinoforms at the head of the failure scarp (SF7), shelf edge deltas (SF8), which increase in height basinward, effectively "heal" relief associated with the shelf edge upper-slope failure. Deltaic deposition increases the grade of the slope to a graded, stable equilibrium profile. The contorted packages (SF9) are interpreted as slumps, which were

likely sourced from failure of the shelf edge deltas (e.g. Mayall et al. 1992; Porębski and Steel 2003).

Base of Slope to Proximal Basin floor

SF10: Chaotic-mounded reflections (mass-transport complexes).---

Description: SF10 comprises a series of mounded packages that are located at the base of slope (Fig. 9). The packages are bound by high-amplitude reflections and are internally chaotic, displaying discontinuous low-amplitude reflections that onlap landward onto the composite erosion surfaces and thin basinward (Fig. 9). The high-amplitude top-surfaces have variable relief (*c.* 50 ms), related to ponding of clinoform bottom-sets (SF8) in the depressions. The basal-surfaces are defined by continuous high-amplitude reflections that link updip to the same stratigraphic surface defining the outer shelf to upper-shelf failure scarps (Fig. 10). Downdip, the basal surfaces may not be strata-concordant, but may instead display considerable relief associated with ramps (c. 50-125 ms) that cross-cut underlying stratigraphy (Fig. 10iii). Although the overall reflection character is chaotic, there are rare examples of fold-thrust systems (especially in downdip areas), and coherent blocks that are *c.* 100-600 m diameter and up to 150 ms (*c.* 205 m) thick. Similar to the shelf-slope system, the volume and frequency of chaotic deposits displays significant lateral variability: (i) the northern area comprises at least five discrete units, with a gross thickness of up to 275 ms (*c.* 375 m), (ii) the central area contains two stacked units that together are up to 250 ms (*c.* 345 m) thick, and (iii) the central-southern comprises a single unit that is up to 75 ms (*c.* 105 m) thick and that pinches out southward (Fig. 9, 12).

Interpretation: We interpret SF10 to represent mass-transport complexes (MTCs) emplaced by debris flow, slump, or slide processes during shelf-margin failure (Dott 1963; Nardin 1979; Nemec 1990). The high-amplitude basal surfaces likely represent kinematic boundary zones upon which the MTCs were transported (*sensu* Butler et al. 2016). The frontal ramps (Fig. 10iii), which forms due to erosion along the basal shear surface, and the transported-blocks together provide kinematic indicators defining the overall transport direction of the MTC (*c.* 127°) (e.g. Frey-Martínez et al. 2006; Steventon et al. 2019).

SF11/12: High-amplitude continuous reflections (slope channels and toe-of-slope fans).---

Description: SF11 and 12 comprises several high-amplitude, moderate- to low-frequency reflections located in the bottomsets of the shelf edge deltas (Fig. 9). There are two main types of high-amplitude seismic facies: (i) SF11, which consists of discontinuous to semi-continuous high-amplitude reflections; and (ii) SF12, which comprises continuous, high-amplitude reflections (Figs. 9, 11). Both seismic facies are offset by normal faults (Fig. 11i). The continuous bottomsets are up to 60 ms (*c.* 83 m) thick on the toe-of-slope and thin to vertical resolution on the lower slope. In strike-section, the moderate-amplitudes on the lower slope change basinward into high-amplitude bottomsets that have a central isochron thick that pinches-out towards its edges into low-amplitude reflections, thus defining a broad, lobate geometry (Fig. 11, B-B'). The discontinuous high-amplitude packages are stratigraphically higher than the lobate packages, and in strike section can be seen to incise into background (low-amplitude) facies (Fig. 11, A-A'). In map-view, SF11 trend subparallel to the shelf edge, merging down-dip into SF12 (Fig. 11ii). The normal faulting was probably caused by underlying salt-withdrawal and displays oblique NNE-SSW amplitude trends to the shelf edge (Fig. 11).

Interpretation: The high-amplitude bottomset reflections (SF12) are interpreted to represent toe-of-slope lobes (fans), supplied by shelf-oblique submarine slope channel-fills (SF11). A similar interpretation is presented for high-amplitude reflections located at the toe-of-slope of prograding shelf edge deltas (Hadler-Jacobsen et al. 2005). Comparable deposits have also been identified in the field (e.g. Steel et al. 2008).

SHELF EDGE TRAJECTORY AND ALONG-STRIKE VARIABILITY

The Paleocene-Eocene margin of the central Santos Basin was defined by a relatively low shelf edge to basin floor relief (see Hadler-Jacobsen et al. 2005), comprising a predominantly progradational to aggradational succession. Overall, the shelf edge trajectory is complex in the north and becomes simpler towards the south with a single falling shelf edge trend. In addition,

the amount of shelf edge progradation decreases southward (*c.* 5.5 km in the north, *c.* 3.0 km in the central, and *c.* 1 km in the southern area). In total, the succession has received a minimum sediment flux (Q) of *c.* 68 $km^3 Myr^{-1}$ over a *c.* 25 Myr time interval. Below we compare the differences in clinoform trajectory and sediment flux between the northern, central, and southern shelf edge.

Northern Shelf edge

The northern shelf edge has the most complex clinoform trajectory, which can be split into three main sequences (Fig. 13). The first (N1) is a falling/flat trajectory, with the shelf edge delta building out from the updip margin of the underlying outer shelf/shelf edge failure scarp (Fig. 13, 9i). The foresets and bottomsets (up to 260 ms, *c.* 358 m) are dominated by shelf edge delta slumps (SF9) and MTCs (SF10), indicating that the margin was unstable at that time. Sequence 1 is separated from 2 by a package defining a distinct backstepping (825 m) of the shelf edge (Fig. 13). Sequence 2 (N2) starts with a relatively short-lived falling/flat trajectory (Fig. 13, North-1), before changing to a rising trajectory. Shelf edge delta slumps (SF9), which are confined to the clinoform foresets, are common in this interval. The bottomset succession is relatively thin (< 50 ms, *ca.* 69 m) when compared to N1 (Fig. 9i). Sequence 3 (N3) is defined by a falling/flat trajectory with notable offlap terminations (Fig. 9i). N3 is characterized by higher amplitudes than N1 and N2, with slope channel-fills (SF11) dominating the foresets and toe-of-slope fans (SF12) occurring in the bottomsets (up to 200 ms, *c.* 275 m). The northern area has a sediment flux of c. 28 $km^3 My^{-1}$ and correlates to the area of maximum thickness on the slope (Fig. 5ii, *c.* 750 ms, *c.*1000 m). The northern area shows correlation between sequence bottomset thickness and clinoform trajectory, with falling/flat trajectories having thicker, and rising trajectories thinner bottomsets (e.g. Steel and Olsen 2002).

Central Shelf edge

The central shelf edge can be split into two main sequences and has a simpler trajectory than the northern shelf edge (Figs. 13, 9ii). Both sequences are falling/flat. Sequence 1 (C1) is composed of shelf edge delta clinoforms (SF7) that infill shelf edge failure scarps, whereas sequence 2 (C2)

is composed of larger shelf edge delta (SF8) clinoforms (Fig. 9ii). The bottomsets of C1 are dominated by upper-slope shelf edge delta slumps (SF9). C2 is thicker, with a mixture of toplap and offlap terminations at the shelf edge, with downlap termination in the bottomsets (Fig. 9ii). Two slope-attached MTCs are present downdip of the central shelf edge. However, it is unlikely that these are related to the preserved clinoform trajectories, because they directly downlap onto the MTCs (Fig. 9i). These MTCs were more likely related to clinoforms that collapsed and are thus no longer preserved. The central area has a lower sediment flux of c. 22 $km^3 Myr^{-1}$ than the northern area and accordingly has a thinner slope succession (Fig. 5ii, up to 500 ms, c. 688m). Although the central area is defined by flat/falling clinoform trajectories, only two MTCs were emplaced on the basin floor; other deep-water deposits, such as channels and lobes, are not observed.

Southern Shelf edge

The southern area has a simple, flat/falling trajectory. A single sequence is identified as most of the clinoform rollover points are difficult to identify and the margin is characterized by a ramp (low grade incline) rather than clinoform geometry. The southern area has the lowest sediment flux of c. 18 $km^3 Myr^{-1}$ (Fig. 5ii, up to 150 ms, c. 205m).

DISCUSSION

The Paleocene-Eocene shelf edge of the central Santos Basin demonstrates significant along-strike variability in terms of shelf-physiography and evolution, and the types of depositional systems occurring on the outer shelf to basin floor. Below we discuss: (i) along-strike variability at the local- and basin-scale, (ii) the driving mechanisms and style of shelf edge collapse and subsequent accretion, and (iii) the controls on sediment partitioning and stratigraphic variability between the shelf edge and deep-water.

Lateral Variability in Shelf edge Physiography

Local variability.---

The central Santos Basin system displays a range of lateral changes in stratigraphic architecture along the *ca.* 90-km-long shelf edge (Fig. 5). These changes are either gradual (tens of kilometres) or abrupt (<1 km), with the larger-scale lateral changes manifested as: (i) gross depositional sequence thinning from north to south, (ii) change in the rate of sediment supply, varying from 28 $km^3 Myr^{-1}$ in the north to 18 $km^3 Myr^{-1}$ in the south, (iii) changes in seismic facies along the shelf (incisional vs. conformable), shelf edge (linear vs. complex failure scarps), slope (degradational vs. progradational), and base of slope (i.e. the relative proportions of MTCs to toe-of-slope fans), and (iv) shelf edge trajectories, changing from complex in the north to simple in the south (Fig. 14). Hence, it is impossible to select a single, representative depositional-dip-oriented section that captures this variability. Below we discuss the depositional and structural controls on this lateral variability.

Dominant sedimentary process.---

The shelf contains extensive NE-SW trending beach ridges, which are aligned sub-parallel to the shelf edge (Fig. 5iv). These beach ridges record deposition within an extensive, wave-dominated coastal depositional system, likely characterized by a wave-dominated delta and flanking shorefaces. These covered large parts of the shelf and extended to the shelf edge, particularly in the north (Fig. 5iv, 8). Wave-dominated shorelines and shelf edge systems have the capacity to efficiently transfer sediment long distances along continental shelves (Snedden et al. 1988). Larger storm surges can incised into shoreface sequences, redistributing sediment offshore by turbulent and mass-wasting processes (e.g. Rogers and Goodbred 2010). Shoreline and shelf systems also have the ability to transfer sediment down-dip from wave-dominated (Fig. 8) deltaic systems to the shelf edge, and along-strike to shelf-slope conduits (e.g. valleys, canyons, gullies; Fig. 7) (Posamentier et al. 1991; Covault and Graham 2010; Hadler-Jacobsen et al. 2010; Peng et al. 2017). Covault and Fildani (2014) also highlight the importance of the shelf width, shelf-slope conduits (or lack of), and littoral drift, in routing sediment to the basin floor. The observed variability may therefore be explained by differential sediment supply across the shelf edge, with fluvial input in the northern area part of the present study area (and areas farther north, outside of our dataset), with this sediment being redistributed along strike by alongshore processes (Fig.

1b). Hence, alongshore rather than fluvial point sources are thought to be the dominant process within this stratigraphic interval, with the northern area interpreted as a mixed wave-dominated fluvial-influenced system, and central/southern areas being more wave-dominated. Our interpretation of the style of shelf depositional system correlates with the observed shelf edge and toe-of-slope deposition, with more sediment bypass in the north (MTCs and toe-of-slope fans) where fluvial input and sediment accumulation rate was highest, decreasing southwards as wave-action preferentially stored sediment along the shelf. This is consistent with other studies that demonstrate effective sediment bypass beyond the slope in fluvial-dominated systems, with wave-dominated systems more likely to promote storage on the shelf (Deibert et al. 2003; Dixon et al. 2012; Cosgrove et al. 2018).

Structure.---

Sediment supply, if high enough, can drive shelf edge progradation even during rising sea-level or highstand conditions (Burgess and Hovius 1998). However, given the complex tectonic regime (transfer zones and salt-tectonics) of the central Santos Basin (Fig. 4, 5iv), it is likely that basin physiography also influenced the observed lateral variability. Structures which may have influenced the inherited topography of the depositional system include; (i) the Albian Gap, restricting sediment input south of the São Paulo transfer zone (Fig. 1), and (ii) spatial variability in subsidence rates during salt-wall rise and withdrawal (Fig. 5iv).

The São Paulo transfer zone marks the boundary between the Albian Gap, a very thick (up to 3 km), salt-related depocenter (Fig.1, see Jackson et al. 2015), and the present study area. One possible scenario is that the Albian Gap captured a large proportion of sediment delivered, along-strike, from high-sediment supply areas in the north of the Santos basin. This major depocenter could have cause much of the southern Santos basin, including this study area, to be sediment starved.

An alternative interpretation is that the São Paulo transfer zone in conjunction with active salt-tectonics created a basin physiography that preferentially focussed the north Santos Basin sediment supply into the northern area of this study. Local salt-structures include an NNE-SSW trending salt wall outboard of the shelf-slope break, and two stocks that underlie the northern and

deeper southern parts of the shelf (Fig 5vi). We suggest that salt tectonics, which was most active during the Late Cretaceous due to sediment loading, caused differential uplift of the shelf, and permitted overall subsidence in the downdip basin. Differential uplift is evidenced by localised incised-valley development along the northern shelf (Fig. 7); such valley-fills are absent in the south. Differential subsidence along the slope to toe-of-slope is demonstrated in the northern area where the supply axis of the shelf edge delta was fixed from approximately Coniacian-Maastrichtian times to the Early Oligocene (a ~50 Myr time interval), while the southern area was sediment starved (Fig 12ii). After the Early Oligocene, this trend switched, with the southern area recording increased sediment input (Figs. 12, 14).

Basin-scale variability.---

In addition to the local variability, the shelf edge also records basin-scale variability. North of the Ilha Grande transfer zone, outside of the study area (Fig. 1), the Paleocene-Eocene shelf edge prograded in a similar manner, with the mid-Eocene scarp displaying a similar morphology (Berton and Vesely 2016). However, the shelf is more fluvially influenced than in this study, with multiple fluvial systems supplying sediment to Paleocene canyons and Eocene slope channel systems. This style of sediment delivery produces both mixed sand-mud and sand-rich (cf. Reading and Richards 1994) basin floor fans and sand-rich MTCs (Ebiwonjumi and Schwartz 2003; Berton and Vesely 2016; Vesely 2016). The Paleocene canyons are up to 300 m deep and are thought to be related to local uplift/relative sea-level fall, correlating with the Maastrichtian-Paleocene (55-59 Ma) horizon mapped in this study (Cobbold et al. 2001; Modica and Brush 2004). However, the shelf still shows signs of being wave-influenced, with arcuate beach ridges imaged on the Eocene shelf (Dixon 2013). The area between the Ilha Grande and São Paulo transfer zones shows a similar pattern to the northern area of the basin, although large Paleocene canyons are not present (Modica and Brush 2004) (Fig. 1). Hadler-Jacobsen et al. (2010) argue that this area was characterized by a predominantly wave-dominated shoreline during the Campanian-Maastrichtian, with shelf transport along-strike supplying canyons and slope channels, with large basin floor fans at their terminus. We postulate that this wave-dominated shoreline continues into the Paleocene-Eocene, forming the northern equivalent of the

strandplain system identified here (Fig. 6i & 8). South of the Merluza transfer zone the sequence is condensed with no evidence of shelf edge deltas (Modica and Brush 2004).

Model and Mechanisms for Collapse

Shelf edge deltas are prone to oversteepening and periodic collapse (Nemec 1990). Previous studies of shelf edge instability demonstrates the process: (i) is indiscriminate of deltaic regime, occurring in wave- (e.g. paleo-Orinoco Delta, Bowman and Johnson 2014), and fluvial-dominated (e.g. Cretaceous Spitsbergen, Nemec et al. 1988) systems, but being rarer in tide-influenced shelf edge deltas (e.g. Cummings et al. 2006), (ii) varies markedly along-strike due to change in the interplay of allo- and autogenic controls (e.g. Olariu and Steel 2009; Zhuo et al. 2018), (iii) is scale-independent, occurring from bed- (e.g. Flint et al. 2011; Hodgson et al. 2018), to system- (e.g. middle-Pliocene, Mississippi Canyon, Mayall et al. 1992), to basin-scale (e.g. this study), and (vi) shows predictable stacking patterns of degradational and later re-establishing sequences. Nevertheless, many shelf edges are relatively stable and only infrequently experience minor instability in the form of soft sediment deformation on the shelf edge, and turbidite/debrite deposition on the slope and basin floor (Plink-Björklund et al. 2001; Mellere et al. 2002).

Many field and subsurface studies have proposed models for predicting stratigraphic and facies changes during shelf edge accretion and collapse, capturing the role of relative sea-level, sediment supply, and inherited structure (e.g. Dixon et al. 2013; Peng et al. 2017; Gomis-Cartesio et al. 2018; Proust et al. 2018). Most of these models only capture 2D end-member or idealised 3D models of a sedimentary system, due to lack of subsurface data resolution and/or coverage, and/or limited exposure in the field. However, most of these models show a systematic pattern of margin development; i.e. an initial period of progradation and then degradation is followed by a later re-establishment phase when relief associated with collapse of the shelf edge/upper-slope is filled or "healed". Studies focusing specifically on along-strike variability are forced to consider a basin in 3D, and identify that time-equivalent intervals along-strike can show vastly differing patterns (e.g. Jones et al. 2015; Madof et al. 2016; Zhuo et al. 2018; Chiarella et al. 2019). These observations therefore suggest the cited 2D-models only have utility where they are related to a similar region of a depositional system (e.g. near the point source of a delta), and breakdown when used to predict changes along-strike. Here we build on these 2D examples by proposing a model capturing all

aspects of basin variability, with focus on along-strike variations in sediment supply, considering high, moderate, and low Q end-members (Fig. 15).

Stage 1: Pre-conditioning.---

Slope failure is primed and triggered by numerous factors (see Locat and Lee 2002; Sultan et al. 2004). In this study, we interpret that slope failure is primed and ultimately triggered by slope oversteepening, which may be enhanced by a pore-pressure increase and associated slope weakening during a period of rapid sediment accumulation. This may have occurred even during periods characterized by rising relative sea-level (i.e. rising trajectories) due to: (i) an increase in sedimentation rate during the middle Eocene, enhanced through renewed onshore uplift and increased sediment flux associated with the Paleocene-Eocene thermal maximum, a period of globally high temperatures, erosion, and sediment discharge to the global oceans (e.g. Harris et al. 2010; Self-Trail et al. 2017), (ii) a lack of conduits (e.g. submarine canyons) to allow sediment bypass, (iii) wave-dominated conditions on the shelf, which promote sediment storage at the shelf edge, and (iv) a lack of evidence for sustained rising trajectories. These factors all suggest that during periods of high shelfal accommodation, the shelf edge prograded and aggraded (i.e. rising trajectory) to a critical slope angle that pre-conditioned the area to failure. Our interpretation is consistent with observations in the northern Santos Basin, where Eocene MTCs are thought to be sourced from highstand and transgressive units (Henriksen et al. 2011; Dixon 2013). This model for slope collapse (or at least pre-conditioning) is consistent with our observation that multiple failure events occurred in the high Q, northern and central area of this study, with the low Q southern part of the margin lacking slope (or ramp) failure and MTC emplacement.

We document multiple Eocene failure events in the Santos Basin, some of which are only locally developed. However, one event seems to be regionally extensive, being broadly coeval along a ~300 km strike-length of the margin (e.g. Berton and Vesely 2016). Given the size and, more specifically, strike extent of the related scarp, we suspect this event formed in response to a regional, allogenic mechanism that acted at the basin-scale. We therefore suggest that a combination of a middle Eocene (40-43 Ma) eustatic sea-level fall (Modica and Brush 2004), and increased contourite current activity associated with the Antarctic Bottom Water, which is thought to have entered the basin from the early Eocene (Barker et al. 1981; Duarte and Viana 2007),

triggered the regional slope failure. Relative sea-level fall could have increased the pore-pressure within shelf edge and slope sediments (Posamentier and Kolla 2003), whereas contourite currents could have had a destabilising effect on an already weak slope (Rebesco et al. 2014). Together, these two mechanisms could have triggered regional failure of the middle Eocene shelf edge and upper-slope.

Stage 2: Degradation of the shelf edge.---

Failure of the outer shelf-to-shelf edge is recorded as MTCs that were deposited on the basin floor. The style of collapse varies across the shelf, with the high Q area in the north recording multiple larger shelf edge failure events, the moderate Q area in the centre recoding two large shelf edge failure events (preserved as two stacked MTC; Fig. 9ii), and the low Q area in the south recording a condensed sequence at the base of slope. The area between the downdip part of the scarp and the onset of MTC deposition (which is essentially a toe-of-slope onlap surface) is a major sediment bypass surface (Fig. 9i & ii) (Stevenson et al. 2015).

Stage 3: Infill of scarp and re-establishment.---

Following shelf edge failure, we observe two principal types of delta: (i) full re-establishment of shelf edge-scale clinoforms, and (ii) partial re-establishment of the upper-slope, with small scale clinoforms (SF7) that evolve into shelf edge scale clinoforms (SF8) (Fig. 9i & ii). Full re-establishment is observed in the high Q areas where the scars are linear. In these cases, we observed progradation of shelf edge scale clinoforms (SF8), with delta-front slumps being deposited on the upper to middle slope. However, more commonly there is only partial re-establishment in both the high and moderate Q areas, where irregular scars in the upper-slope are infilled by upper-slope slumps (SF9) and small deltas (SF7). Similar depositional patterns are observed in the field. For example, in Cretaceous pro-delta sequences in eastern Spitsbergen, Norway, scarps are initially infilled by slump and debris flow deposits, followed by mud-rich turbidites that coarsen upwards (Nemec et al. 1988; Onderdonk and Midtkandal 2010). In the paleo-Orinoco pro-delta, upper-slope facies successions demonstrate a mixture of relatively large shelf edge failure (*c.* 50 m thick) with delta-front blocks, and smaller packages (metre-scale) of thin-bedded turbidites and slumps

(Bowman and Johnson 2014). The Berton and Vesely (2016) seismic-based study of the Eocene succession in the northern Santos Basin documents only full re-establishment. We suggest the difference in shelf edge re-establishment may be related to the variation in deltaic processes from more fluvially-influenced in the north of the Santos Basin (Berton and Vesely 2016), to more wave-dominated in the south (i.e. this study).

Once gradients on the upper-slope stabilised, overlying deltaic were able to re-establish themselves, eventually prograding basinward and increasing in size to become shelf edge-scale clinothem packages. This suggests that, even after Stage 2, the shelf edge was still unstable, with re-establishment a process of smaller degradational events allowing infill and stabilisation of the irregular upper-slope morphology.

Stratigraphic Prediction on Degradational Margins

Missing trajectories.---

In many examples in the north of our study area, flat/falling trajectories are correlated with shelf incision, offlapping geometries, and high-amplitude reflections relating to toe-of-slope and basin floor fan deposits. Hadler-Jacobsen et al. (2005) interprets the systems as a sediment overfilled margin, with larger basin floor fans relating to flat/falling trajectories. MTCs are interpreted to be sourced from highstand/transgressive units (Henriksen et al. 2011; Dixon et al. 2012). These interpretations agree with our own results, which show that falling/flat trajectories are related to thicker bottomsets, rising trajectories are related to thinner bottomsets, and MTCs represent remobilised rising trajectories.

Use of trajectory analysis has generally focused on examples that demonstrate the complete, or near complete, lateral and vertical migration of a break-in-slope. Generally rising, flat, and falling trends can be used to predict delivery of sand-grade material to the basin floor, and hence predict reservoir presence (e.g. Steel and Olsen 2002). In shorelines, these migration pathways can be well-preserved, with modification through incision by later channels or canyons (e.g. Tesson et al. 2000). Similarly, many shelf edges have little or only minor shelf edge degradation (e.g. Johannessen and Steel 2005). However, on shelf edges prone to multiple delta-front

collapse phases (i.e. this study), preservation of the full record of shelf edge trajectories is low (e.g. Gomis-Cartesio et al. 2018). This poses difficulties in using trajectory methods including; incomplete preservation, diachroneity, and irregular upper-slope gradients that may preferentially produce trajectories that do not represent conventional interpretations (e.g. falling trajectory = falling relative sea-level). However, with increased seismic data coverage (i.e. 3D rather than 2D) we can improve our understanding and appreciation of stratigraphic completeness, and the impact this has on our assessment of spatial variations in margin trajectory (see Mahon et al. 2015).

As shown in this study, degradational margins can include an under-representation of rising trajectories (due to remobilisation as MTCs) in the preserved shelf edge trajectory. These "missing" trajectories may cause misinterpretation of sediment partition from the shelf to basin floor by either: (i) overrepresentation of falling/flat trajectories (Fig. 13), (ii) underpredicting rising trajectories and potential bias towards flat/falling trends that tend to be more stable, or (iii) underprediction of falling/flat trajectories in particular stratigraphic intervals, due to remobilisation during large-scale shelf edge failure. Therefore, we should also consider missing trajectories (i.e. MTCs & smaller slumps) when analysing the stratigraphic development of degradation-prone shelf edges.

Our interpretation suggest that MTC emplacement occurred mainly during times of rising trajectories, in contrast to that predicted by conventional sequence-stratigraphic models (e.g. Weimer 1990; Kolla and Perlmutter 1993) that predict slope failure and MTC deposition preferentially occur during falling-stage to early lowstand systems tracts (falling trajectories). Our observations thus agree with other studies hypothesising that MTCs can be emplaced during any phase of the sea-level cycle, during both rising and falling relative sea-level (e.g. Maslin et al. 1998; Posamentier and Kolla 2003; Brothers et al. 2013), along with similar observations from other basin types (e.g. Dalla Valle et al. 2013). These results demonstrate the importance of understanding missing trajectories and the driving mechanisms behind shelf edge failure, particularly when trying to apply conventional sequence stratigraphic concepts.

Lateral variability and non-uniqueness.---

In addition to predicting sediment partitioning in 2D, this study has shown the importance of along-strike variability in stratigraphic prediction for shelf edge deltas, and for slope and toe-of-slope deposits. Yet, the concept of strike variability in sequence stratigraphy is not new. Lateral variability in stacking patterns demonstrate how systems-tract-based models can be unreliable as a predictive tool (Wehr 1993; Martinsen and Helland-Hansen 1995). More recently, Burgess and Prince (2015) use numerical models to show the potential for non-uniqueness, demonstrating that: (i) sequence bounding unconformities can be generated by both accommodation controls (i.e. relative sea-level fall) and variations in sediment transport rates, and (ii) similar shoreline/shelf edge trajectories can be created with different accommodation and sediment transport rates. Similarly, maximum flooding/transgressive surfaces may not be present across the shelf and do not always represent a single, coeval, correlative conformity, as demonstrated in moving hinge conceptual models (Madof et al. 2016).

The examples shown here from offshore Brazil are consistent with some of the predictions made above. For example, there is significant lateral variability in margin stacking pattern from north to south (Fig. 14). Without considering lateral changes or having access to three-dimensional data one could erroneously infer: (i) highstand (HST), falling-stage (FSST), lowstand (LST), and transgressive (TST) systems tracts in the northern area, (ii) FSST, LST, and TST in the central area, and (iii) TST or HST in the southern area (Figs. 9, 12, 14). In addition to stratal stacking patterns, this study shows lateral variability in key bounding surfaces. In particular, shelf incision and formation of an erosion surface (see Fig. 7i) in the north but not in south, possibly reflecting along-strike changes in differential subsidence, rather than sediment supply and accumulation (see Burgess and Prince 2015). If we were to take a solely two-dimensional approach, we may erroneously relate incision of the northern shelf (Fig. 7) to a period of relative sea-level fall and lowstand. If so, we may interpret the erosion surface as a regionally developed sequence boundary, and draw similarly incorrect conclusions regarding the nature, timing, and distribution of sediment bypass beyond the shelf edge to the slope and basin floor. With our 3D control we can almost certainly say that this is a local, not a regional, unconformity, being the product of local fluvial incision. One surface that is extensive across the entire Santos Basin is the Early Oligocene flooding surface (Modica and Brush 2004), thought to be generated from eustatic sea-

level rise. However, the resulting backstepping of the shelf is also approximately coeval with reorganisation of drainage away from the Santos and into the Campos basin; hence the flooding surface is most likely a product of both relative sea-level rise and decreased sediment flux.

The Paleocene-Eocene shelf edge is an example of how sediment supply and structure may locally modify eustatic sea-level fluctuations and shows the importance of considering along-strike variability and degradational processes before applying a specific sequence-stratigraphic model. Regardless of how sophisticated sequence-stratigraphic models become, a basin-by-basin approach to understanding depositional systems is essential such that the likely role of allogenic and autogenic controls can be understood.

CONCLUSIONS

(i) The Paleocene-Eocene of the central Santos Basin is a wave-dominated shelf edge, with minor fluvial influence. The shelf edge is prone to failure and has produced a complex distribution of slope and toe-of-slope sedimentation. We build upon the Modica and Brush (2004) basin-wide review to show the Paleocene-Eocene deltaic system, and potentially prospective toe-of-slope fans extends farther south than previously thought.

(ii) The Paleocene-Eocene interval has shown to be prone to periodic shelf edge collapse. We interpret the principal mechanism of repetitive failure to be related to oversteepening of the delta-front during periods of high sediment supply and shelfal accommodation (e.g. rising relative sea-level). For the mid-Eocene scarp, which represents a coeval catastrophic collapse from the central area of this study to the Cabo Frio High, we suggest a combination of eustatic sea-level fall and increased bottom-current activity.

(iii) We propose a 3D model for accretion styles on degradational shelf edges, which incorporates lateral variability. The model distinguishes the changes in accretionary style and deposition from low to high sediment supplied shelf edges, and can be split into three phases, Stage 1: pre-conditioning; Stage 2: degradation and emplacement of the collapsed shelf edge; and Stage 3: infilling of the upper-slope scarp and delta re-establishment.

(iv) Trajectory analysis has shown that falling/flat trajectories correlate with thicker bottomset and preserved rising trajectories correlate with thinner bottomsets, which is a generally accepted trend. However, we have also highlighted the importance of recognising MTCs and smaller upper-slope slumps as "missing" trajectories and incorporating these into interpretations of shelf edge storage vs bypass.

(v) Lateral (along-strike) variability in shelf edge, slope and toe-of-slope is the norm in both ancient and modern systems. We have demonstrated locally how over tens of kilometres the style of shelf edge accretion changes and interpret this variability to be predominantly caused by basin margin physiography and variations in sediment supply. Through confirmation with other Santos Basin studies we show that this variability extends to the north and south, with variations in depocenter thicknesses, topset process regime and deep-water sedimentation.

(vi) This well constrained 3D example demonstrates the importance of building along-strike variability directly into predictive sequence stratigraphic, trajectory, and stratigraphic-forward models. Nonetheless, a basin-by-basin approach to understanding along-strike variability, will greatly aid in the characterisation of depositional systems and their allogenic and autogenic controls.

Acknowledgement

We thank the reviewers Jinyu Zhang and Ashley Harris for their constructive feedback which greatly improved the final submission, together with John Southard, Melissa Lester, Andrea Fildani and Peter Burgess for editorial handling. Thanks to Domenico Chiarella for his correspondence and feedback on the initial preprint. We express thanks to Webster Mohriak and the Brazilian National Agency of Petroleum, Natural Gas and Biofuels for providing access to data. Thanks to Schlumberger and ffA Geoteric for software donations.

REFERENCES

ADAMS, E.W., AND SCHLAGER, W., 2000, Basic types of submarine slope curvature: Journal of Sedimentary Research, v. 70, p. 814-828.

BARKER, P.F., CARLSON, R.L., JOHNSON, D.A., CEPEK, P., COULBOURN, W., GAMBÔA, L.A., HAMILTON, N., MELO, U., PUJOL, C., AND SHOR, A.N., 1981, Deep sea drilling project leg 72: Southwest Atlantic paleocirculation and Rio Grande Rise tectonics: Geological Society of America, Bulletin, v. 92, p. 294-309.

BERTON, F., AND VESELY, F.F., 2016, Stratigraphic evolution of Eocene clinoforms from northern Santos Basin, offshore Brazil: Evaluating controlling factors on shelf-margin growth and deep-water sedimentation: Marine and Petroleum Geology, v. 78, p. 356-372.

BOWMAN, A.P., AND JOHNSON, H.D., 2014, Storm-dominated shelf-edge delta successions in a high accommodation setting: The palaeo-Orinoco Delta (Mayaro Formation), Columbus Basin, South-East Trinidad: Sedimentology, v. 61, p. 792-835.

BROTHERS, D.S., LUTTRELL, K.M., AND CHAYTOR, J.D., 2013, Sea-level-induced seismicity and submarine landslide occurrence: Geology, v. 41, p. 979-982.

BURGESS, P.M., 2016, The future of the sequence stratigraphy paradigm: Dealing with a variable third dimension: Geology, v. 44, p. 335-336.

BURGESS, P.M., AND HOVIUS, N., 1998, Rates of delta progradation during highstands: consequences for timing of deposition in deep-marine systems: Journal of the Geological Society of London, v. 155, p. 217-222.

BURGESS, P.M., AND PRINCE, G.D., 2015, Non-unique stratal geometries: implications for sequence stratigraphic interpretations: Basin Research, v. 27, p. 351-365.

BUTLER, R.W., EGGENHUISEN, J.T., HAUGHTON, P., AND MCCAFFREY, W.D., 2016, Interpreting syndepositional sediment remobilization and deformation beneath submarine gravity flows; a kinematic boundary layer approach: Journal of the Geological Society of London, v. 173, p. 46-58.

CARVAJAL, C., STEEL, R., AND PETTER, A., 2009, Sediment supply: the main driver of shelf-margin growth: Earth-Science Reviews, v. 96, p. 221-248.

CARVAJAL, C.R., AND STEEL, R.J., 2006, Thick turbidite successions from supply-dominated shelves during sea-level highstand: Geology, v. 34, p. 665-668.

CATUNEANU, O., 2006, Principles of sequence stratigraphy, Elsevier, Amsterdam.

CHANG, H.K., KOWSMANN, R.O., FIGUEIREDO, A.M.F., AND BENDER, A., 1992, Tectonics and stratigraphy of the East Brazil Rift system: an overview: Tectonophysics, v. 213, p. 97-138.

CHIARELLA, D., LONGHITANO, S.G., AND TROPEANO, M., 2019, Different stacking patterns along an active fold-and-thrust belt—Acerenza Bay, Southern Apennines (Italy): Geology, v. 47, p. 139-142.

CLEMSON, J., CARTWRIGHT, J., AND BOOTH, J., 1997, Structural segmentation and the influence of basement structure on the Namibian passive margin: Journal of the Geological Society of London, v. 154, p. 477-482.

COBBOLD, P.R., MEISLING, K.E., AND MOUNT, V.S., 2001, Reactivation of an obliquely rifted margin, Campos and Santos basins, southeastern Brazil: American Association of Petroleum Geologists (AAPG) bulletin, v. 85, p. 1925-1944.

COSGROVE, G.I., HODGSON, D.M., POYATOS-MORÉ, M., MOUNTNEY, N.P., AND MCCAFFREY, W.D., 2018, Filter Or Conveyor? Establishing Relationships Between Clinoform Rollover Trajectory, Sedimentary Process Regime, and Grain Character Within Intrashelf Clinothems, Offshore New Jersey, USA: Journal of Sedimentary Research, v. 88, p. 917-941.

COVAULT, J.A., AND FILDANI, A., 2014, Continental shelves as sediment capacitors or conveyors: source-to-sink insights from the tectonically active Oceanside shelf, southern California, USA: Geological Society of London, Memoirs, v. 41, p. 315-326.

COVAULT, J.A., AND GRAHAM, S.A., 2010, Submarine fans at all sea-level stands: Tectono-morphologic and climatic controls on terrigenous sediment delivery to the deep sea: Geology, v. 38, p. 939-942.

CUMMINGS, D.I., ARNOTT, R.W.C., AND HART, B.S., 2006, Tidal signatures in a shelf-margin delta: Geology, v. 34, p. 249-252.

DALLA VALLE, G., GAMBERI, F., ROCCHINI, P., MINISINI, D., ERRERA, A., BAGLIONI, L., AND TRINCARDI, F., 2013, 3D seismic geomorphology of mass transport complexes in a foredeep basin: Examples from the Pleistocene of the Central Adriatic Basin (Mediterranean Sea): Sedimentary Geology, v. 294, p. 127-141.

DAVISON, I., 2007, Geology and tectonics of the South Atlantic Brazilian salt basins: Geological Society of London, Special Publications, v. 272, p. 345-359.

DAVISON, I., ANDERSON, L., AND NUTTALL, P., 2012, Salt deposition, loading and gravity drainage in the Campos and Santos salt basins: Geological Society of London, Special Publications, v. 363, p. 159-174.

DEIBERT, J., BENDA, T., LØSETH, T., SCHELLPEPER, M., AND STEEL, R., 2003, Eocene clinoform growth in front of a storm-wave-dominated shelf, Central Basin, Spitsbergen: no significant sand delivery to deepwater areas: Journal of Sedimentary Research, v. 73, p. 546-558.

DIXON, J., STEEL, R., AND OLARIU, C., 2012, Shelf edge delta regime as a predictor of deep-water deposition: Journal of Sedimentary Research, v. 82, p. 681-687.

DIXON, J.F., 2013, Shelf edge deltas: stratigraphic complexity and relationship to deep-water deposition: Univeristy of Texas at Austin, Electronic Theses and Dissertations.

DIXON, J.F., STEEL, R.J., AND OLARIU, C., 2013, A model for cutting and healing of deltaic mouth bars at the shelf edge: mechanism for basin-margin accretion: Journal of Sedimentary Research, v. 83, p. 284-299.

DOTT, R., 1963, Dynamics of subaqueous gravity depositional processes: American Association of Petroleum Geologists (AAPG) Bulletin, v. 47, p. 104-128.

DUARTE, C.S., AND VIANA, A.R., 2007, Santos Drift System: stratigraphic organization and implications for late Cenozoic palaeocirculation in the Santos Basin, SW Atlantic Ocean: Geological Society of London, Special Publications, v. 276, p. 171-198.

EBIWONJUMI, F.R., AND SCHWARTZ, D., 2003, Eocene Depositional Model for the Brazil Santos Basin in the Vicinity of the BS-4—NE Discovery: Shelf Margin Deltas and Linked Down Slope Petroleum Systems–Global Significance and Future Exploration Potential, v. 23.

FLINT, S., AND, HODGSON, D., SPRAGUE, A., BRUNT, R., VAN DER MERWE, W., FIGUEIREDO, J., PRÉLAT, A., BOX, D., DI CELMA, C., AND KAVANAGH, J., 2011, Depositional architecture and sequence stratigraphy of the Karoo basin floor to shelf edge succession, Laingsburg depocentre, South Africa: Marine and Petroleum Geology, v. 28, p. 658-674.

FREY-MARTÍNEZ, J., CARTWRIGHT, J., AND JAMES, D., 2006, Frontally confined versus frontally emergent submarine landslides: a 3D seismic characterisation: Marine and Petroleum Geology, v. 23, p. 585-604.

GALLOWAY, W.E., 1998, Siliciclastic slope and base-of-slope depositional systems: component facies, stratigraphic architecture, and classification: American Association of Petroleum Geologists (AAPG) bulletin, v. 82, p. 569-595.

GOMIS-CARTESIO, L.E., POYATOS-MORÉ, M., HODGSON, D.M., AND FLINT, S.S., 2018, Shelf-margin clinothem progradation, degradation and readjustment: Tanqua depocentre, Karoo Basin (South Africa): Sedimentology, v. 65, p. 809-841.

GUERRA, M.C., AND UNDERHILL, J.R., 2012, Role of halokinesis in controlling structural styles and sediment dispersal in the Santos Basin, offshore Brazil: Geological Society of London, Special Publications, v. 363, p. 175-206.

HADLER-JACOBSEN, F., GROTH, A., HEARN, R.E., LIESTØL, F.M., WOOD, L., SIMO, T., AND ROSEN, N., 2010, Controls on and expressions of submarine fan genesis within a high accommodation margin setting, Santos Basin, Brazil—A high-resolution seismicstratigraphic and geomorphic case study: Seismic Imaging of Depositional and Geomorphic Systems: Gulf Coast Section SEPM Foundation Annual Bob F. Perkins Research Conference Proceedings, p. 572-615.

HADLER-JACOBSEN, F., JOHANNESSEN, E., ASHTON, N., HENRIKSEN, S., JOHNSON, S., AND KRISTENSEN, J., 2005, Submarine fan morphology and lithology distribution: a predictable function of sediment delivery, gross shelf-to-basin relief, slope gradient and basin topography: Geological Society of London, Petroleum Geology Conference Series, p. 1121-1145.

HAMPSON, G.J., 2016, Towards a sequence stratigraphic solution set for autogenic processes and allogenic controls: Upper Cretaceous strata, Book Cliffs, Utah, USA: Journal of the Geological Society of London, v. 173, p. 817-836.

HAQ, B.U., HARDENBOL, J., AND VAIL, P.R., 1987, Chronology of fluctuating sea levels since the Triassic: Science, v. 235, p. 1156-1167.

HARRIS, A.D., MILLER, K.G., BROWNING, J.V., SUGARMAN, P.J., OLSSON, R.K., CRAMER, B.S., AND WRIGHT, J.D., 2010, Integrated stratigraphic studies of Paleocene–lowermost Eocene sequences, New Jersey Coastal Plain: Evidence for glacioeustatic control: Paleoceanography, v. 25, p. 1-18.

HELLAND-HANSEN, W., AND GJELBERG, J.G., 1994, Conceptual basis and variability in sequence stratigraphy: a different perspective: Sedimentary Geology, v. 92, p. 31-52.

HELLAND-HANSEN, W., AND MARTINSEN, O.J., 1996, Shoreline trajectories and sequences: description of variable depositional-dip scenarios: Journal of Sedimentary Research, v. 66, p. 670-688.

HELLAND-HANSEN, W., AND HAMPSON, G., 2009, Trajectory analysis: concepts and applications: Basin Research, v. 21, p. 454-483.

HENRIKSEN, S., HELLAND-HANSEN, W., AND BULLIMORE, S., 2011, Relationships between shelf-edge trajectories and sediment dispersal along depositional dip and strike: a different approach to sequence stratigraphy: Basin Research, v. 23, p. 3-21.

HODGSON, D., BROWNING, J., MILLER, K., HESSELBO, S., POYATOS-MORÉ, M., MOUNTAIN, G., AND PROUST, J.-N., 2018, Sedimentology, stratigraphic context, and implications of Miocene intrashelf bottomset deposits, offshore New Jersey: Geosphere, v. 14, p. 95-114.

HUNT, D., AND TUCKER, M.E., 1992, Stranded parasequences and the forced regressive wedge systems tract: deposition during base-level'fall: Sedimentary Geology, v. 81, p. 1-9.

JACKSON, C.A.-L., 2012, The initiation of submarine slope failure and the emplacement of mass transport complexes in salt-related minibasins: A three-dimensional seismic-reflection case study from the Santos Basin, offshore Brazil: Geological Society of America Bulletin, v. 124, p. 746-761.

JACKSON, C.A.-L., GRUNHAGEN, H., HOWELL, J.A., LARSEN, A.L., ANDERSSON, A., BOEN, F., AND GROTH, A., 2010, 3D seismic imaging of lower delta-plain beach ridges: lower Brent Group, northern North Sea: Journal of the Geological Society of London, v. 167, p. 1225-1236.

JACKSON, C.A.-L., JACKSON, M.P., AND HUDEC, M.R., 2015, Understanding the kinematics of salt-bearing passive margins: A critical test of competing hypotheses for the origin of the Albian Gap, Santos Basin, offshore Brazil: Bulletin, v. 127, p. 1730-1751.

JOHANNESSEN, E.P., AND STEEL, R.J., 2005, Shelf-margin clinoforms and prediction of deepwater sands: Basin Research, v. 17, p. 521-550.

JONES, G.E., HODGSON, D.M., AND FLINT, S.S., 2015, Lateral variability in clinoform trajectory, process regime, and sediment dispersal patterns beyond the shelf-edge rollover in exhumed basin margin-scale clinothems: Basin Research, v. 27, p. 657-680.

KARNER, G., AND GAMBÔA, L., 2007, Timing and origin of the South Atlantic pre-salt sag basins and their capping evaporites: Geological Society of London, Special Publications, v. 285, p. 15-35.

KARNER, G.D., AND DRISCOLL, N.W., 1999, Tectonic and stratigraphic development of the West African and eastern Brazilian Margins: insights from quantitative basin modelling: Geological Society of London, Special Publications, v. 153, p. 11-40.

KOLLA, V., AND PERLMUTTER, M., 1993, Timing of turbidite sedimentation on the Mississippi Fan: American Association of Petroleum Geologists (AAPG) Bulletin, v. 77, p. 1129-1141.

LOCAT, J., AND LEE, H.J., 2002, Submarine landslides: advances and challenges: Canadian Geotechnical Journal, v. 39, p. 193-212.

MACEDO, J., 1989, Evolução tectônica da Bacia de Santos e áreas continentais adjacentes: Petrobras Geosciences Newsletter, v. 3, p. 159-173.

MADOF, A.S., HARRIS, A.D., AND CONNELL, S.D., 2016, Nearshore along-strike variability: Is the concept of the systems tract unhinged?: Geology, v. 44, p. 315-318.

MAHON, R.C., SHAW, J.B., BARNHART, K.R., HOBLEY, D.E., AND MCELROY, B., 2015, Quantifying the stratigraphic completeness of delta shoreline trajectories: Journal of Geophysical Research: Earth Surface, v. 120, p. 799-817.

MARFURT, K.J., SCHEET, R.M., SHARP, J.A., AND HARPER, M.G., 1998, Suppression of the acquisition footprint for seismic sequence attribute mapping: Geophysics, v. 63, p. 1024-1035.

MARTINSEN, O.J., AND HELLAND-HANSEN, W., 1995, Strike variability of clastic depositional systems: Does it matter for sequence-stratigraphic analysis?: Geology, v. 23, p. 439-442.

MASLIN, M., MIKKELSEN, N., VILELA, C., AND HAQ, B., 1998, Sea-level-and gas-hydrate-controlled catastrophic sediment failures of the Amazon Fan: Geology, v. 26, p. 1107-1110.

MAYALL, M., YEILDING, C., OLDROYD, J., PULHAM, A., AND SAKURAI, S., 1992, Facies in a Shelf edge Delta--An Example from the Subsurface of the Gulf of Mexico, Middle Pliocene, Mississippi Canyon, Block 109 (1): American Association of Petroleum Geologists (AAPG) Bulletin, v. 76, p. 435-448.

MCMURRAY, L.S., AND GAWTHORPE, R.L., 2000, Along-strike variability of forced regressive deposits: late Quaternary, northern Peloponnesos, Greece: Geological Society of London, Special Publications, v. 172, p. 363-377.

MEISLING, K.E., COBBOLD, P.R., AND MOUNT, V.S., 2001, Segmentation of an obliquely rifted margin, Campos and Santos basins, southeastern Brazil: American Association of Petroleum Geologists (AAPG) bulletin, v. 85, p. 1903-1924.

MELLERE, D., PLINK-BJÖRKLUND, P., AND STEEL, R., 2002, Anatomy of shelf deltas at the edge of a prograding Eocene shelf margin, Spitsbergen: Sedimentology, v. 49, p. 1181-1206.

MITCHUM, R.M., VAIL, P.R., AND SANGREE, J.B., 1977, Seismic stratigraphy and global changes of sea level: Part 6. Stratigraphic interpretation of seismic reflection patterns in depositional sequences: Section 2. Application of seismic reflection configuration to stratigraphic interpretation.

MODICA, C.J., AND BRUSH, E.R., 2004, Postrift sequence stratigraphy, paleogeography, and fill history of the deep-water Santos Basin, offshore southeast Brazil: American Association of Petroleum Geologists (AAPG) bulletin, v. 88, p. 923-945.

MOHRIAK, W., NEMČOK, M., AND ENCISO, G., 2008, South Atlantic divergent margin evolution: rift-border uplift and salt tectonics in the basins of SE Brazil: Geological Society of London, Special Publications, v. 294, p. 365-398.

MOREIRA, J.L.P., MADEIRA, C., GIL, J., AND MACHADO, M.P., 2007, bacia de Santos: Boletim de Geociencias da PETROBRAS, v. 15, p. 531-549.

MUTO, T., STEEL, R.J., AND SWENSON, J.B., 2007, Autostratigraphy: a framework norm for genetic stratigraphy: Journal of Sedimentary Research, v. 77, p. 2-12.

NARDIN, T.R., 1979, A review of mass movement processes sediment and acoustic characteristics, and contrasts in slope and base-of-slope systems versus canyon-fan-basin floor systems: SEPM Special Publication.

NEAL, J., AND ABREU, V., 2009, Sequence stratigraphy hierarchy and the accommodation succession method: Geology, v. 37, p. 779-782.

NEAL, J.E., ABREU, V., BOHACS, K.M., FELDMAN, H.R., AND PEDERSON, K.H., 2016, Accommodation succession (δA/δS) sequence stratigraphy: observational method, utility and insights into sequence boundary formation: Journal of the Geological Society of London, v. 173, p. 803-816.

NEMEC, W., 1990, Aspects of sediment movement on steep delta slopes: Special Publication, International Association of Sedimentologists, Coarse-grained deltas, v. 10, p. 29-73.

NEMEC, W., STEEL, R., GJELBERG, J., COLLINSON, J., PRESTHOLM, E., AND OXNEVAD, I., 1988, Anatomy of collapsed and re-established delta front in Lower Cretaceous of eastern Spitsbergen: gravitational sliding and sedimentation processes: American Association of Petroleum Geologists (AAPG) Bulletin, v. 72, p. 454-476.

OLARIU, C., AND STEEL, R.J., 2009, Influence of point-source sediment-supply on modern shelf-slope morphology: implications for interpretation of ancient shelf margins: Basin Research, v. 21, p. 484-501.

ONDERDONK, N., AND MIDTKANDAL, I., 2010, Mechanisms of collapse of the Cretaceous Helvetiafjellet Formation at Kvalvågen, eastern Spitsbergen: Marine and Petroleum Geology, v. 27, p. 2118-2140.

OTVOS, E.G., 2000, Beach ridges-definitions and significance: Geomorphology, v. 32, p. 83-108.

PARTYKA, G., GRIDLEY, J., AND LOPEZ, J., 1999, Interpretational applications of spectral decomposition in reservoir characterization: The Leading Edge, v. 18, p. 353-360.

PATRUNO, S., HAMPSON, G.J., AND JACKSON, C.A.L., 2015, Quantitative characterisation of deltaic and subaqueous clinoforms: Earth-Science Reviews, v. 142, p. 79-119.

PATRUNO, S., AND HELLAND-HANSEN, W., 2018, Clinoform systems: Review and dynamic classification scheme for shorelines, subaqueous deltas, shelf edges and continental margins: Earth-Science Reviews, v. 185, p. 202-233.

PENG, Y., STEEL, R.J., AND OLARIU, C., 2017, Transition from storm wave-dominated outer shelf to gullied upper slope: The mid-Pliocene Orinoco shelf margin, South Trinidad: Sedimentology, v. 64, p. 1511-1539.

PLINK-BJÖRKLUND, P., MELLERE, D., AND STEEL, R.J., 2001, Turbidite variability and architecture of sand-prone, deep-water slopes: Eocene clinoforms in the Central Basin, Spitsbergen: Journal of Sedimentary Research, v. 71, p. 895-912.

PORĘBSKI, S.J., AND STEEL, R.J., 2003, Shelf-margin deltas: their stratigraphic significance and relation to deepwater sands: Earth-Science Reviews, v. 62, p. 283-326.

POSAMENTIER, H., ERSKINE, R., AND MITCHUM, R., 1991, Models for submarine-fan deposition within a sequence-stratigraphic framework, Seismic facies and sedimentary processes of submarine fans and turbidite systems, Springer, p. 127-136.

POSAMENTIER, H.W., ALLEN, G.P., JAMES, D.P., AND TESSON, M., 1992, Forced regressions in a sequence stratigraphic framework: concepts, examples, and exploration significance (1): American Association of Petroleum Geologists (AAPG) bulletin, v. 76, p. 1687-1709.

POSAMENTIER, H.W., AND KOLLA, V., 2003, Seismic geomorphology and stratigraphy of depositional elements in deep-water settings: Journal of Sedimentary Research, v. 73, p. 367-388.

PRATHER, B.E., O'BYRNE, C., PIRMEZ, C., AND SYLVESTER, Z., 2017, Sediment partitioning, continental slopes and base-of-slope systems: Basin Research, v. 29, p. 394-416.

PROUST, J.-N., POUDEROUX, H., ANDO, H., HESSELBO, S.P., HODGSON, D.M., LOFI, J., RABINEAU, M., AND SUGARMAN, P.J., 2018, Facies architecture of Miocene subaqueous clinothems of the New Jersey passive margin: Results from IODP-ICDP Expedition 313: Geosphere.

READING, H.G., AND RICHARDS, M., 1994, Turbidite systems in deep-water basin margins classified by grain size and feeder system: American Association of Petroleum Geologists (AAPG) bulletin, v. 78, p. 792-822.

REBESCO, M., HERNÁNDEZ-MOLINA, F.J., VAN ROOIJ, D., AND WÅHLIN, A., 2014, Contourites and associated sediments controlled by deep-water circulation processes: state-of-the-art and future considerations: Marine Geology, v. 352, p. 111-154.

ROGERS, K.G., AND GOODBRED, S.L., 2010, Mass failures associated with the passage of a large tropical cyclone over the Swatch of No Ground submarine canyon (Bay of Bengal): Geology, v. 38, p. 1051-1054.

ROSS, W., HALLIWELL, B., MAY, J., WATTS, D., AND SYVITSKI, J., 1994, Slope readjustment: a new model for the development of submarine fans and aprons: Geology, v. 22, p. 511-514.

SAENZ, C.T., HACKSPACHER, P., NETO, J.H., IUNES, P., GUEDES, S., RIBEIRO, L., AND PAULO, S., 2003, Recognition of Cretaceous, Paleocene, and Neogene tectonic reactivation through apatite fission-track analysis in Precambrian areas of southeast Brazil: association with the opening of the south Atlantic Ocean: Journal of South American Earth Sciences, v. 15, p. 765-774.

SELF-TRAIL, J.M., ROBINSON, M.M., BRALOWER, T.J., SESSA, J.A., HAJEK, E.A., KUMP, L.R., TRAMPUSH, S.M., WILLARD, D.A., EDWARDS, L.E., AND POWARS, D.S., 2017, Shallow marine response to global climate change during the Paleocene-Eocene Thermal Maximum, Salisbury Embayment, USA: Paleoceanography, v. 32, p. 710-728.

SNEDDEN, J.W., NUMMEDAL, D., AND AMOS, A.F., 1988, Storm-and fairweather combined flow on the central Texas continental shelf: Journal of Sedimentary Research, v. 58, p. 580-595.

STEEL, R., AND OLSEN, T., 2002, Clinoforms, clinoform trajectories and deepwater sands: Gulf Coast SEPM 22nd Research Conference.

STEEL, R.J., CARVAJAL, C., PETTER, A.L., UROZA, C., HAMPSON, G., BURGESS, P., AND DALRYMPLE, R., 2008, Shelf and shelf-margin growth in scenarios of rising and falling sea level: Recent advances in models of siliciclastic shallow-marine stratigraphy, v. 90, p. 47e71.

STEVENSON, C.J., JACKSON, C.A.-L., HODGSON, D.M., HUBBARD, S.M., AND EGGENHUISEN, J.T., 2015, Deep-water sediment bypass: Journal of Sedimentary Research, v. 85, p. 1058-1081.

STEVENTON, M.J., JACKSON, C.A.L., HODGSON, D.M., AND JOHNSON, H.D., 2019, Strain analysis of a seismically-imaged mass-transport complex (MTC), offshore Uruguay: Basin Research.

SULTAN, N., COCHONAT, P., CANALS, M., CATTANEO, A., DENNIELOU, B., HAFLIDASON, H., LABERG, J., LONG, D., MIENERT, J., AND TRINCARDI, F., 2004, Triggering mechanisms of slope instability processes and sediment failures on continental margins: a geotechnical approach: Marine Geology, v. 213, p. 291-321.

TESSON, M., POSAMENTIER, H.W., AND GENSOUS, B., 2000, Stratigraphic organization of late pleistocene deposits of the western part of the Golfe du Lion shelf (Languedoc shelf), Western Mediterranean Sea, using high-resolution seismic and core data: American Association of Petroleum Geologists (AAPG) Bulletin, v. 84, p. 119-150.

TORSVIK, T.H., ROUSSE, S., LABAILS, C., AND SMETHURST, M.A., 2009, A new scheme for the opening of the South Atlantic Ocean and the dissection of an Aptian salt basin: Geophysical Journal International, v. 177, p. 1315-1333.

VAIL, P.R., MITCHUM JR, R., AND THOMPSON, S., 1977, Seismic stratigraphy and global changes of sea level: Part 3. Relative changes of sea level from Coastal Onlap: section 2. Application of seismic reflection Configuration to Stratigrapic Interpretation.

VAN BEMMEL, P.P., AND PEPPER, R.E., 2000, Seismic signal processing method and apparatus for generating a cube of variance values, Google Patents.

VAN WAGONER, J.C., MITCHUM, R., CAMPION, K., AND RAHMANIAN, V., 1990, Siliciclastic Sequence Stratigraphy in Well Logs, Cores, and Outcrops: Concepts for High-Resolution Correlation of Time and Facies: AMerican Association of Petroleum Geologists (AAPG) Methods in Exploration Series v. 7.

VESELY, F.F., 2016, Seismic expression of depositional elements associated with a strongly progradational shelf margin: northern Santos Basin, southeastern Brazil: Brazilian Journal of Geology, v. 46, p. 585-603.

WEHR, F., 1993, Effects of Variations in Subsidence and Sediment Supply on Parasequence Stacking Patterns: Chapter 14: Recent Developments in Siliciclastic Sequence Stratigraphy, v. M 58: Siliciclastic Sequence Stratigraphy: Recent Developments and Applications.

WEIMER, P., 1989, Sequence stratigraphy of the Mississippi Fan (Plio-Pleistocene), Gulf of Mexico: Geo-Marine Letters, v. 9, p. 185-272.

WEIMER, P., 1990, Sequence Stratigraphy, Facies Geometries, and Depositional History of the Mississippi Fan, Gulf of Mexico (1): American Association of Petroleum Geologists (AAPG) bulletin, v. 74, p. 425-453.

WILLIAMS, B.G., AND HUBBARD, R.J., 1984, Seismic stratigraphic framework and depositional sequences in the Santos Basin, Brazil: Marine and Petroleum Geology, v. 1, p. 90-104.

ZHANG, J., BURGESS, P.M., GRANJEON, D., AND STEEL, R., 2019, Can sediment supply variations create sequences? Insights from stratigraphic forward modelling: Basin Research, v. 31, p. 274-289.

ZHUO, H., WANG, Y., SUN, Z., WANG, Y., XU, Q., HOU, P., WANG, X., ZHAO, Z., ZHOU, W., AND XU, S., 2018, Along-strike variability in shelf-margin morphology and accretion pattern: An example from the northern margin of the South China Sea: Basin Research, v. 31, p. 431-460.

FIGURES LEGEND

Figure 1: Schematic block-diagrams (left = fluvial-dominated, right = wave-dominated) depicting the along-strike variability of degradational continental margins, showing conceptual end-members (i) sediment starved/low sediment flux (Q), (ii) moderate Q, and (iii) high Q.

Figure 2: Location map of the Santos Basin, study area in the red box, with gross-depositional elements from the mid-Eocene modified from Modica and Brush (2004). NE-SW depositional trend of the Eocene shelf edge deltas and related MTCs and turbidites. Both the Atlanta and Oliva fields sit within the Eocene toe-of-slope. Note study area index map depicting, northern, central, and southern areas.

Figure 3: Tectono-stratigraphy of the Santos Basin collated from (Meisling et al. 2001; Modica and Brush 2004; Duarte and Viana 2007; Moreira et al. 2007; Jackson 2012) and observations from this study's dataset. Global sea-level curve from (Haq et al. 1987). SDM = Serra do Mar mountain range.

Figure 4: (i) Dip-oriented seismic section within the central area of the survey outlining shelf edge deltas of the Jureia progradational phase and related slope-attached MTC, (ii) dip-oriented geosection, (iii) strike-oriented seismic section through the late Cretaceous to Eocene base of slope sequence (iv) strike-oriented geosection. Note thinning of the Maastrichtian-Paleocene to Early Oligocene to the south. Stratigraphic ages are estimated from Modica and Brush (2004); Davison (2007); Berton and Vesely (2016).

Figure 5: (i) Index map with locations of Maastrichtian-Paleocene and Early Oligocene shelf-slope breaks, (ii) time-thickness map (isochron, TST = true stratigraphic thickness) between the Maastrichtian-Paleocene and Early Oligocene; note thickness decrease at the shelf edge and slope from north to south, (iii) Maastrichtian-Paleocene time-structure map, (iv) variance extraction of

the Maastrichtian-Paleocene showing significant shelf edge failure scarp in the north, an Aptian salt wall to the south and an isolated diapir along with linear sets (see Fig.7) on the shelf (v) Early Oligocene time-structure map, (vi) variance extraction of the Early Oligocene, note that the shelf edge failure scarp has been infilled by progradation of subsequent shelf edge deltas.

Figure 6: Northern shelf, (i) dip-oriented seismic section through the northern shelf highlighting sequences of mid-shelf deltas (SF6), related beach-ridges (SF4), and incised valley fill (SF2), (ii) strike-oriented seismic section; note thinning of the sequence towards the salt-related structural high, (iii) time-thickness map (isochron, TST = true stratigraphic thickness) between the toplap and downlap surfaces in the dip-oriented section, note significant thinning towards the shelf edge, (iv) variance extraction of the downlap surface, highlighting salt-related structures and beach-ridges (SF4).

Figure 7: Beach-ridges/strandplain seismic facies, (i) dip-oriented seismic section through beach ridges and swales (SF4) note alternating high and low amplitudes, (ii) strike-section; note high-amplitude and continuity of the ridge, (iii) RMS amplitude and spectral decomposition extractions through the ridges and swales; note linear plan-view form, discordances between sets and crescent shaped reflections interpreted as lagoons, (iv) spectral decomposition extraction 50 ms below the Early Oligocene showing a distributary channel system incising into the strandplain, (v) modern-day Pariba do Sul strandplain/beach ridge system (source Google Earth), inset map showing modern day river in flood with along-strike sediment transport (source NASA Earth Observatory); note scales similar to ancient depositional system shown in this study.

Figure 8: (i/ii/ii) Seismic sections of the relationship between incised valleys (SF2) and related distributary channels (SF3), (iv) spectral decomposition extraction from 150 ms below the Early Oligocene, showing the spatial relationship between incised valleys, inter-valley areas, and distributary channel-fills.

Figure 9: Dip seismic sections demonstrating the along-strike variability of the shelf edge from north to south, (i) northern-type section (high Q) with many progradational shelf edge delta (SF8) sequences; note upper-slope slumps (SF9), MTCs (SF10), slope channels (SF11), and toe-of-slope fans (SF12) downdip of the shelf edge, (ii) central-type section (moderate Q) with a significant headwall scarp (see Fig. 11), slope-attached MTCs (SF10), proto-shelf edge deltas (SF7), and shelf edge deltas (SF8), (iii) southern-type section (low Q), thin/condensed section. Note N1/2/3 and C1/2 related to sequences outlined in section 5.

Figure 10: MTCs in the central region of the study area, (i) variance extraction from the mid-Eocene failure scarp, demonstrating that the scrap is a zone of deformation rather than a single plane, (ii) dip seismic section through the scarp zone; note minor slumping on the upper-slope (SF9), (iii) dip seismic section through 2 seismically imaged MTCs (SF10), note high-amplitude basal-shear zones (BSZ), a frontal-ramp, and the internal chaotic seismic texture of the MTCs.

Figure 11: Toe-of-slope fan system in northern region of the study area, (i/ii) spectral decomposition and RMS amplitude extraction from clinoform labelled in Fig. 9i; note the elongate lobate geometry (SF12) at the toe-of-slope manifested as a high-amplitude response in a background of low-amplitudes and along-strike amplitudes on the slope, (iii) A-A' proximal strike seismic section showing isolated high-amplitude reflections interpreted as slope channels (SF11), (iv) B-B' medial strike seismic section through the central axis of the fan; note isochron thick in the centre, thinning towards the fan fridges, (v) C-C' distal strike seismic section with salt-related normal faulting.

Figure 12: Strike variability of the Maastrichtian-Paleocene to Early Oligocene shelf edge, note time-thickness decrease in all seismic sections from north (high Q) to south (low Q), (i) shelf edge strike seismic section with failure scarps appearing as irregular incisional features, (ii) slope strike section recording significant deltaic input in the north where the sediment supply axis has remained fixed through-out the time-interval, with significant stratigraphic thinning towards the south, (iii) toe-of-slope seismic strike section with toe-of-slope fans (SF12) and MTCs (SF10)

dominant in the north, MTCs dominant in the central area, and a condensed sequence recorded in the south.

Figure 13: Clinoform trajectories from mid-Eocene to Early Oligocene demonstrate a complex signature in the north with rising, falling, and flat trajectories, in the central area the shelf edge is characterized by a predominantly falling trajectory, and in the south the shelf edge is either falling or clinoform rollover points are absent/below seismic resolution. North-2 and Central-1 represent the northern and central dip-sections in Fig.9, others can be found in the supplementary material.

Figure 14: Synthesis of observations from high, to moderate, to low Q. Note significant differences in clinoform trajectory signature and related deep-water deposits along the shelf edge.

Figure 15: Conceptual model of along-strike variability and potential facies architectures to expect from high, moderate, and low Q shelf edge settings.

Table 1: Summary table of observed seismic facies and interpretations

Table 2: Morphometric parameters observed in the Paleocene-Eocene seismic facies outlined in Table 1, VR = vertical resolution.

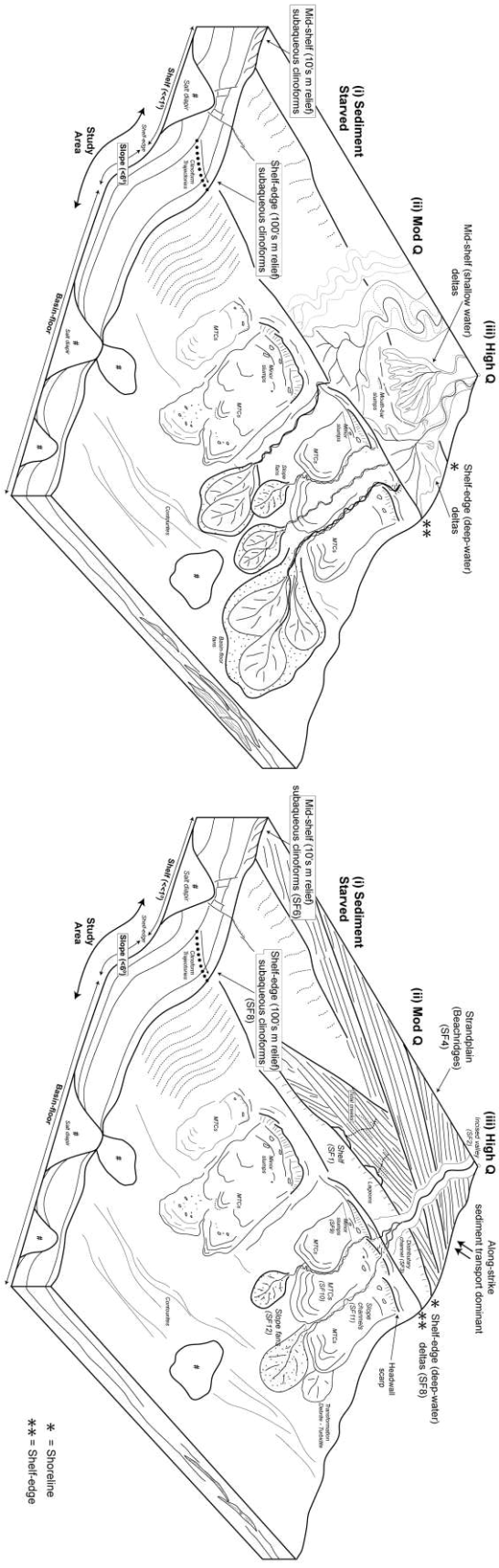
(i) Sediment Starved
(ii) Mod Q
(iii) High Q
Mid-shelf (10's m relief) subaqueous clinoforms
Shelf-edge (100's m relief) subaqueous clinoforms
Mid-shelf (shallow water) deltas
Shelf-edge (deep-water) deltas
Study Area
Shelf (<<1°)
Slope (<6°)
Basin-floor
Strandplain (Beachridges) (SF4)
Shelf (SF1)
Along-strike sediment transport dominant
Shelf-edge (deep-water) deltas (SF8)
Headwall scarp
Mid-shelf (10's m relief) subaqueous clinoforms (SF6)
Shelf-edge (100's m relief) subaqueous clinoforms (SF8)
* = Shoreline
** = Shelf-edge

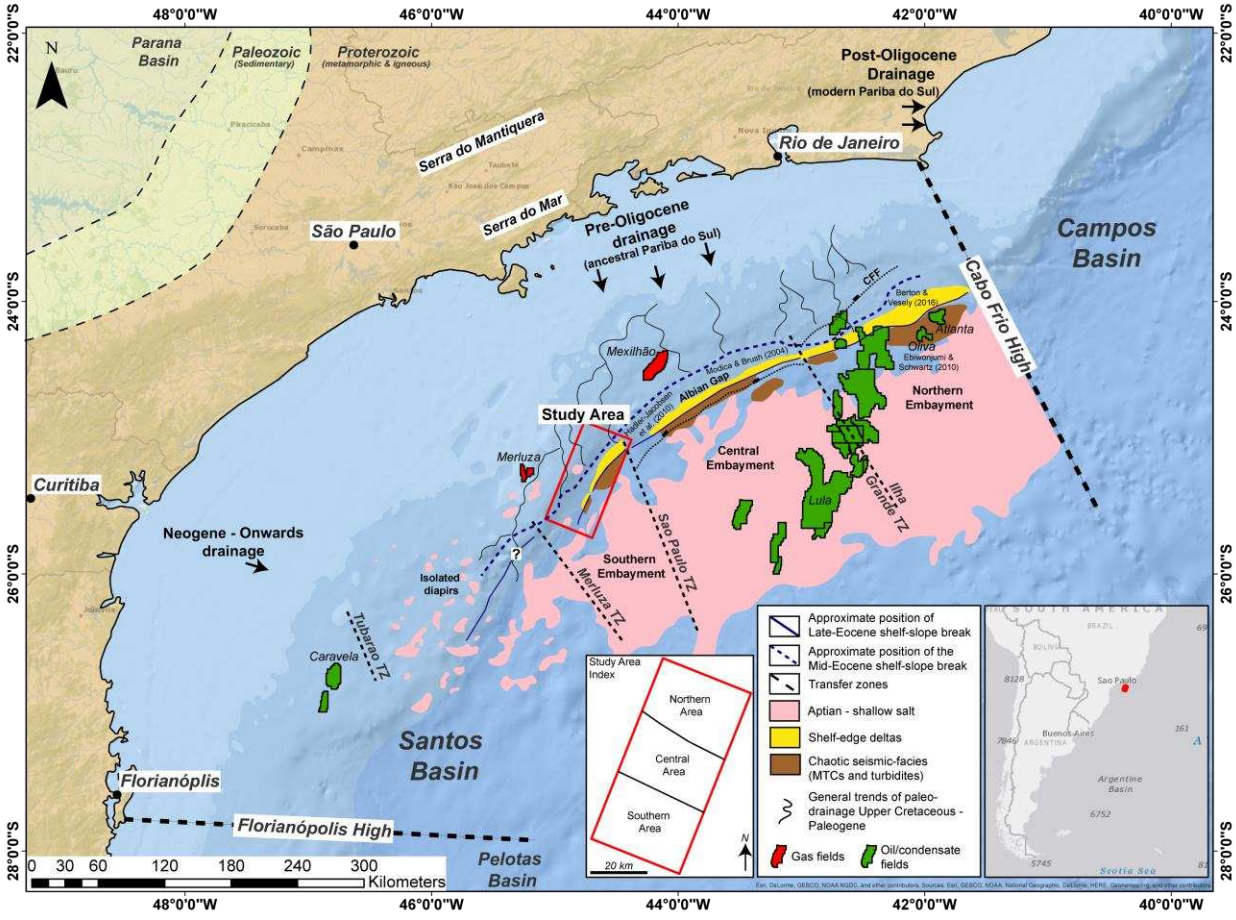
48°0'0"W
46°0'0"W
44°0'0"W
42°0'0"W
40°0'0"W
22°0'0"S
24°0'0"S
26°0'0"S
28°0'0"S
N
Parana Basin
Paleozoic (Sedimentary)
Proterozoic (metamorphic & igneous)
Post-Oligocene Drainage (modern Pariba do Sul)
Rio de Janeiro
Serra do Mantiquera
Serra do Mar
São Paulo
Pre-Oligocene drainage (ancestral Pariba do Sul)
Campos Basin
Cabo Frio High
CFF
Berton & Vesely (2016)
Atlanta
Oliva
Ebiwonjumi & Schwartz (2010)
Mexilhão
Moreira & Bruhn (2004)
Albian Gap
Northern Embayment
Study Area
Merluza
Central Embayment
Curitiba
Lula
Ilha Grande TZ
Neogene - Onwards drainage
Isolated diapirs
Southern Embayment
São Paulo TZ
Merluza TZ
Tubarão TZ
Caravela
Santos Basin
Florianópolis
Florianópolis High
Pelotas Basin
0 30 60 120 180 240 300 Kilometers
Study Area Index
Northern Area
Central Area
Southern Area
20 km
Approximate position of Late-Eocene shelf-slope break
Approximate position of the Mid-Eocene shelf-slope break
Transfer zones
Aptian - shallow salt
Shelf-edge deltas
Chaotic seismic-facies (MTCs and turbidites)
General trends of paleo-drainage Upper Cretaceous - Paleogene
Gas fields
Oil/condensate fields
SOUTH AMERICA
Sao Paulo
Buenos Aires
Argentine Basin
Scotia Sea

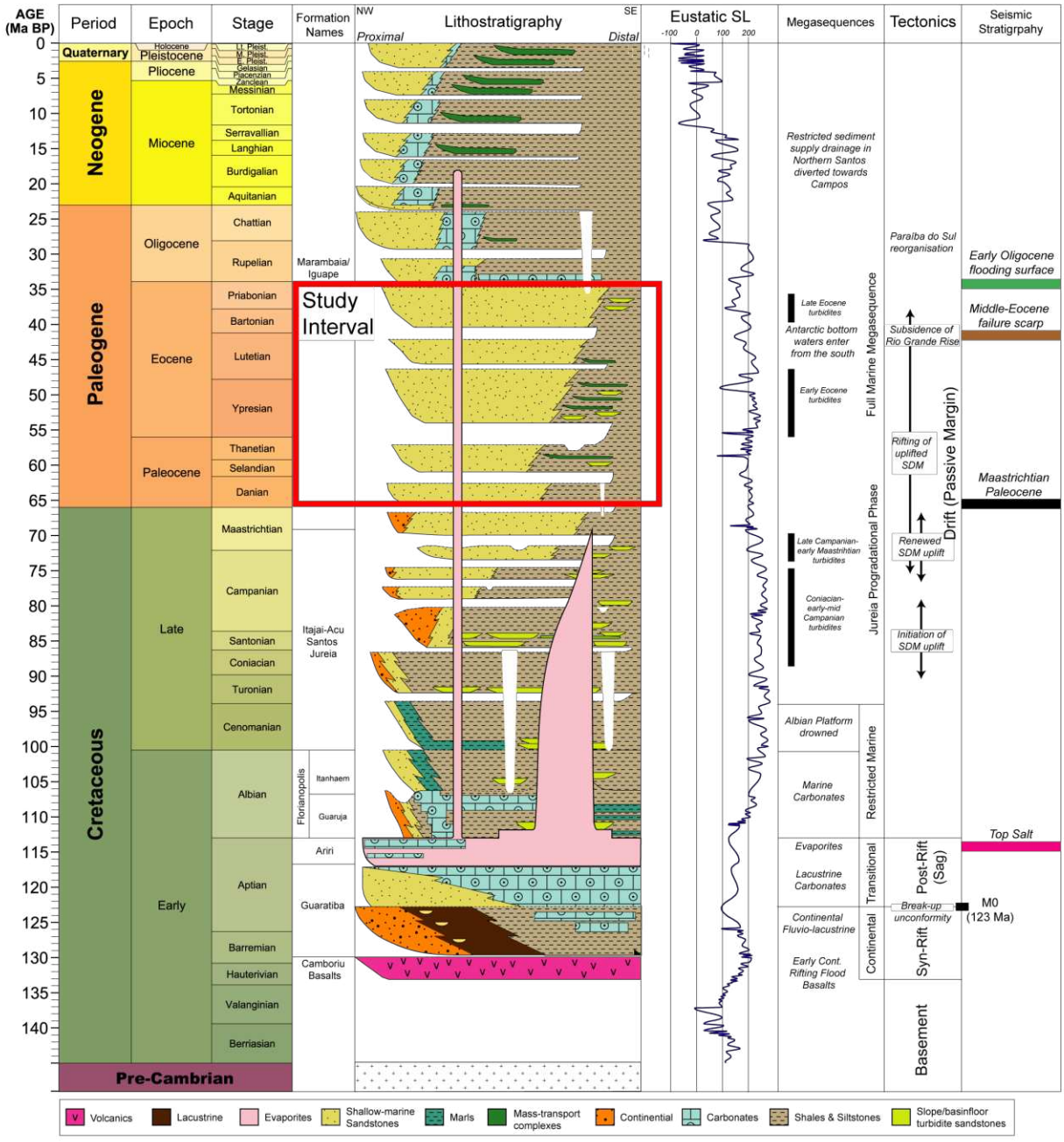
AGE (Ma BP)
Period
Epoch
Stage
Formation Names
NW
Proximal
Lithostratigraphy
Distal
SE
Eustatic SL
-100
0
100
200
Megasequences
Tectonics
Seismic Stratigrpahy
Quaternary
Pleistocene
Holocene
U. Pleist.
M. Pleist.
E. Pleist.
Neogene
Pliocene
Gelasian
Piacenzian
Zanclean
Miocene
Messinian
Tortonian
Serravallian
Langhian
Burdigalian
Aquitanian
Paleogene
Oligocene
Chattian
Rupelian
Marambaia/ Iguape
Eocene
Priabonian
Bartonian
Lutetian
Ypresian
Study Interval
Paleocene
Thanetian
Selandian
Danian
Cretaceous
Late
Maastrichtian
Campanian
Santonian
Coniacian
Turonian
Cenomanian
Itajai-Acu Santos Jureia
Early
Albian
Florianopolis
Itanhaem
Guaruja
Aptian
Ariri
Guaratiba
Barremian
Hauterivian
Valanginian
Berriasian
Camboriu Basalts
Pre-Cambrian
Restricted sediment supply drainage in Northern Santos diverted towards Campos
Late Eocene turbidites
Antarctic bottom waters enter from the south
Early Eocene turbidites
Full Marine Megasequence
Late Campanian-early Maastrihtian turbidites
Coniacian-early-mid Campanian turbidites
Jureia Progradational Phase
Albian Platform drowned
Marine Carbonates
Restricted Marine
Evaporites
Lacustrine Carbonates
Transitional
Continental Fluvio-lacustrine
Early Cont. Rifting Flood Basalts
Continental
Paraíba do Sul reorganisation
Subsidence of Rio Grande Rise
Rifting of uplifted SDM
Renewed SDM uplift
Initiation of SDM uplift
Drift (Passive Margin)
Post-Rift (Sag)
Break-up unconformity
Syn-Rift
Basement
Early Oligocene flooding surface
Middle-Eocene failure scarp
Maastrichtian Paleocene
Top Salt
M0 (123 Ma)
Volcanics
Lacustrine
Evaporites
Shallow-marine Sandstones
Marls
Mass-transport complexes
Continential
Carbonates
Shales & Siltstones
Slope/basinfloor turbidite sandstones

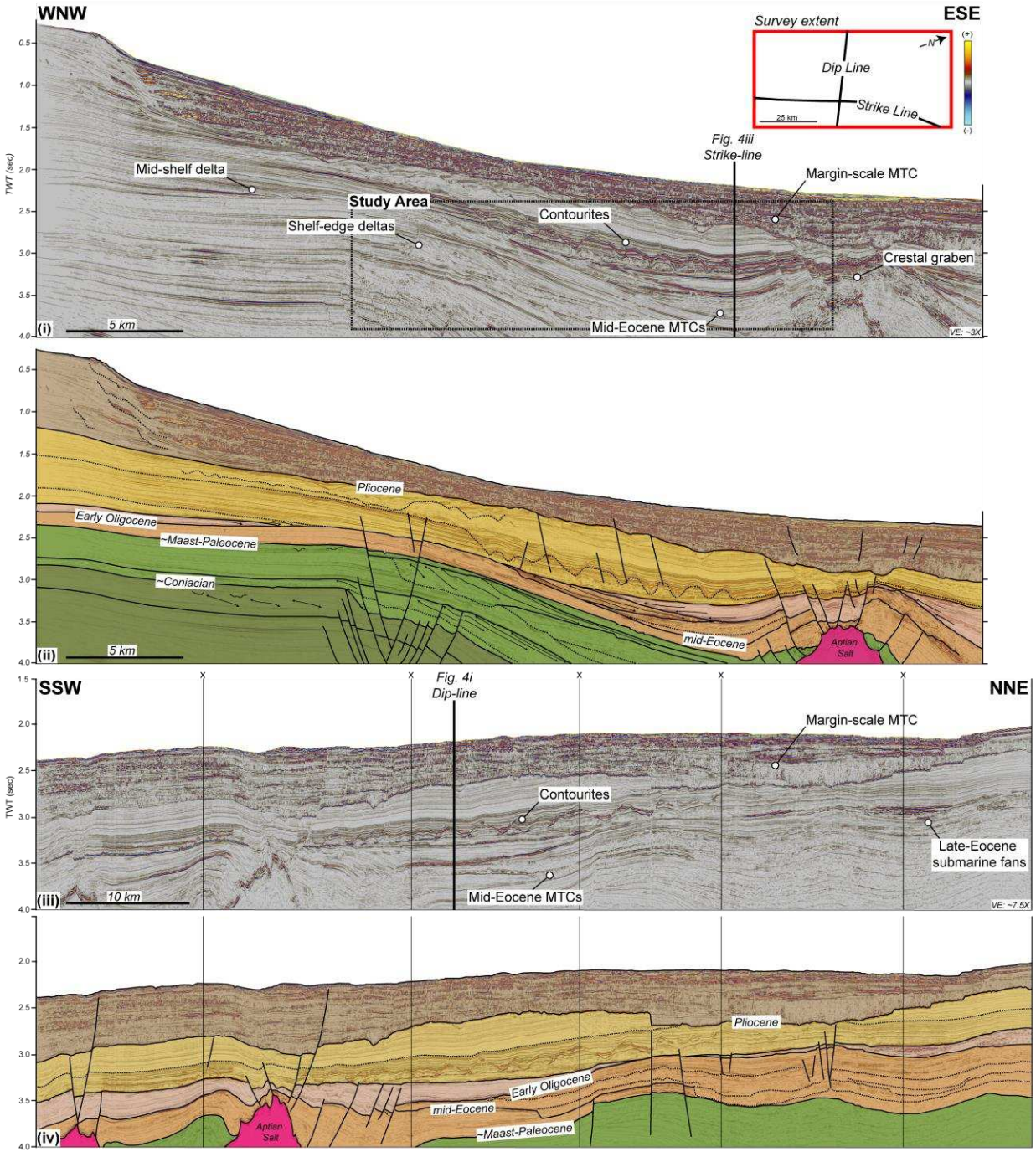
WNW
ESE
Survey extent
Dip Line
Strike Line
25 km
Fig. 4iii
Strike-line
Mid-shelf delta
Study Area
Shelf-edge deltas
Contourites
Margin-scale MTC
Crestal graben
Mid-Eocene MTCs
(i)
5 km
VE: ~3X
TWT (sec)
Pliocene
Early Oligocene
~Maast-Paleocene
~Coniacian
mid-Eocene
Aptian Salt
(ii)
5 km
SSW
NNE
Fig. 4i
Dip-line
Margin-scale MTC
Contourites
Late-Eocene submarine fans
Mid-Eocene MTCs
(iii)
10 km
VE: ~7.5X
Pliocene
Early Oligocene
mid-Eocene
~Maast-Paleocene
Aptian Salt
(iv)

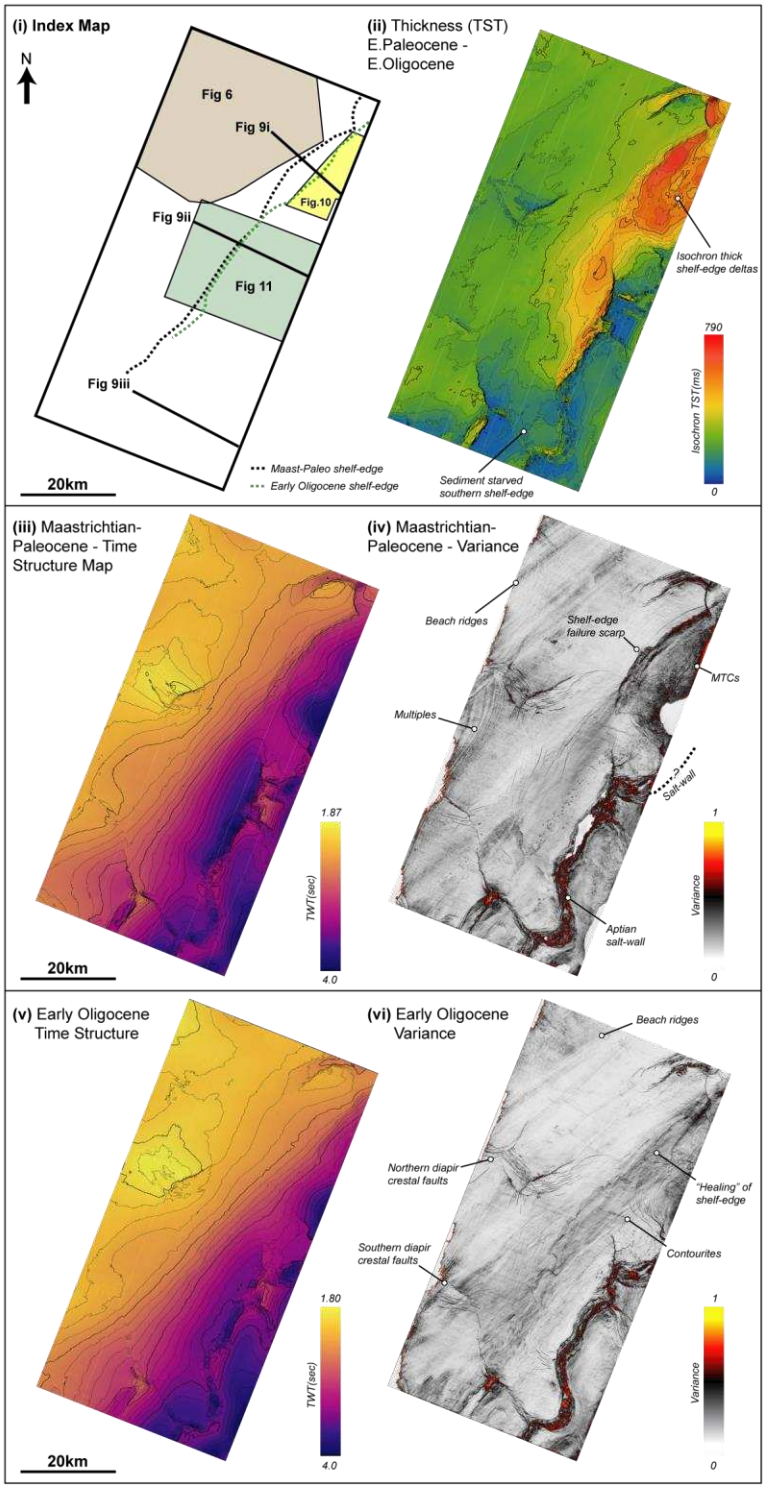
(i) Index Map
N
Fig 6
Fig 9i
Fig.10
Fig 9ii
Fig 11
Fig 9iii
Maast-Paleo shelf-edge
Early Oligocene shelf-edge
20km
(ii) Thickness (TST) E.Paleocene - E.Oligocene
Isochron thick shelf-edge deltas
Sediment starved southern shelf-edge
790
Isochron TST(ms)
0
(iii) Maastrichtian-Paleocene - Time Structure Map
1.87
TWT(sec)
4.0
20km
(iv) Maastrichtian-Paleocene - Variance
Beach ridges
Shelf-edge failure scarp
MTCs
Multiples
Salt-wall
Aptian salt-wall
1
Variance
0
(v) Early Oligocene Time Structure
1.80
TWT(sec)
4.0
20km
(vi) Early Oligocene Variance
Beach ridges
Northern diapir crestal faults
"Healing" of shelf-edge
Southern diapir crestal faults
Contourites
1
Variance
0

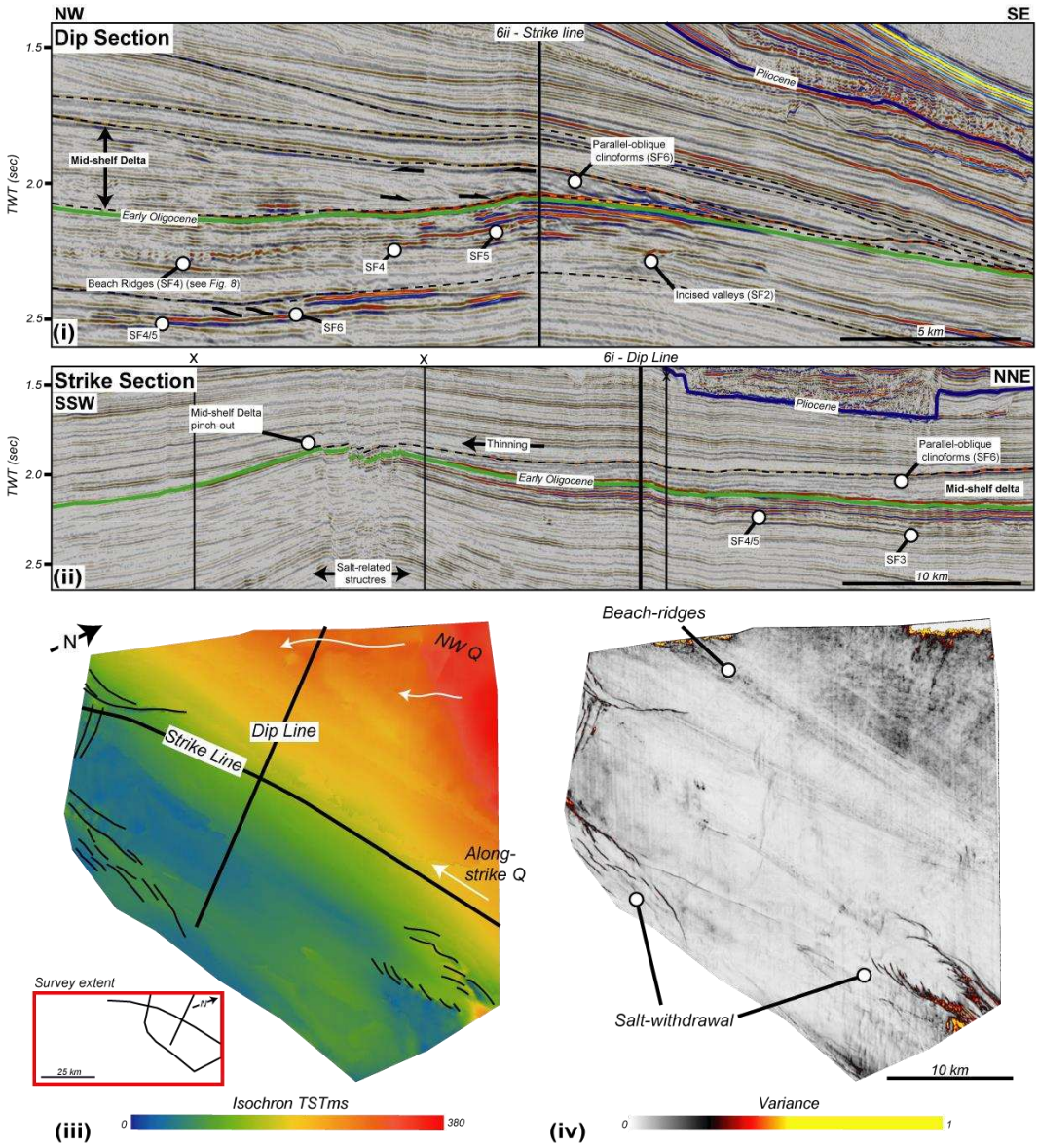
NW
SE
Dip Section
6ii - Strike line
Pliocene
Parallel-oblique clinoforms (SF6)
Mid-shelf Delta
Early Oligocene
SF4
SF5
Beach Ridges (SF4) (see Fig. 8)
Incised valleys (SF2)
SF4/5
SF6
5 km
TWT (sec)
1.5
2.0
2.5
(i)
X
X
6i - Dip Line
Strike Section
SSW
NNE
Mid-shelf Delta pinch-out
Thinning
Early Oligocene
Pliocene
Parallel-oblique clinoforms (SF6)
Mid-shelf delta
SF4/5
SF3
Salt-related structres
10 km
(ii)
N
NW Q
Dip Line
Strike Line
Along-strike Q
Survey extent
25 km
Isochron TSTms
0
380
(iii)
Beach-ridges
Salt-withdrawal
10 km
Variance
0
1
(iv)

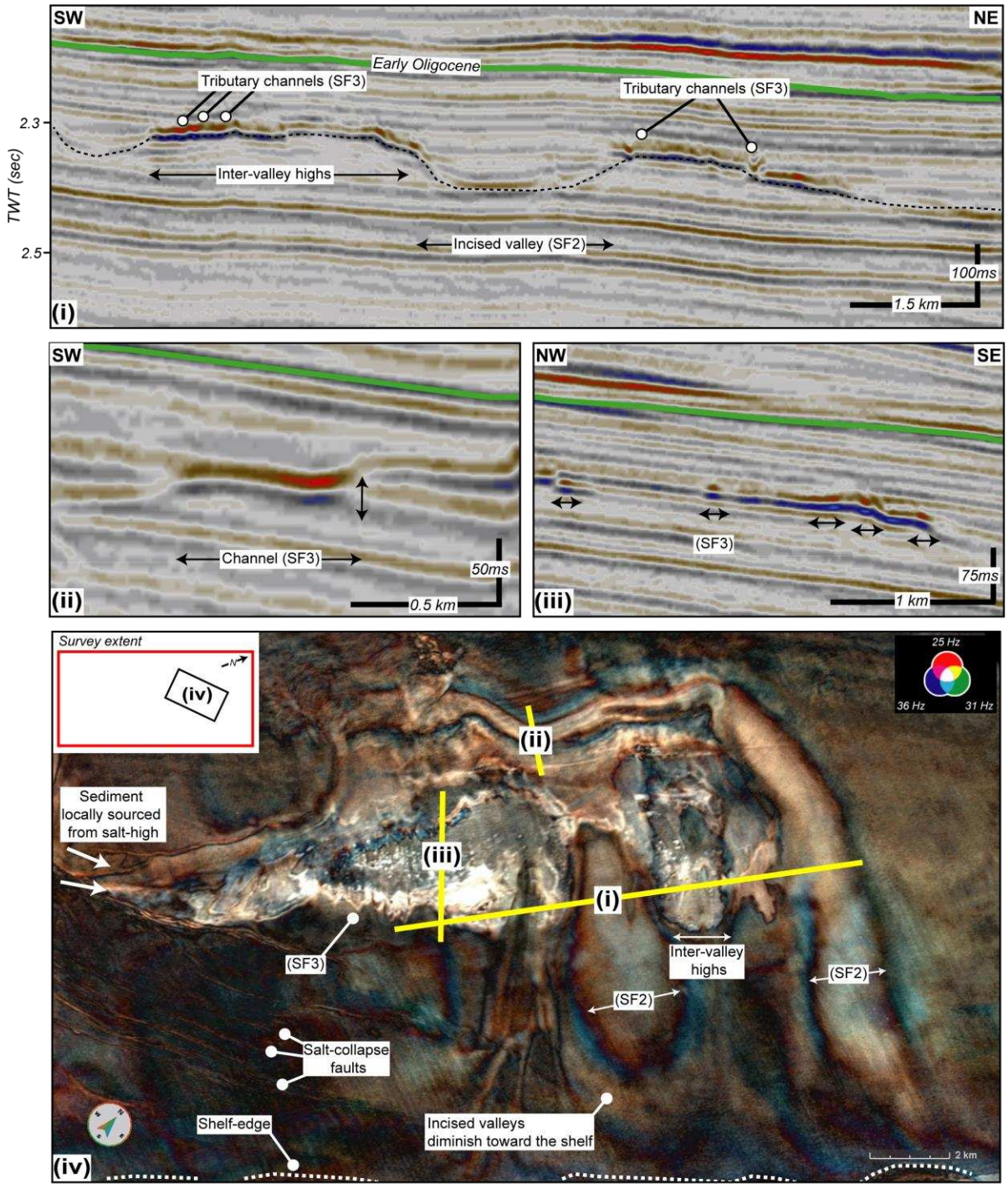
SW
NE
Early Oligocene
Tributary channels (SF3)
Tributary channels (SF3)
2.3
TWT (sec)
2.5
Inter-valley highs
Incised valley (SF2)
100ms
1.5 km
(i)
SW
Channel (SF3)
50ms
0.5 km
(ii)
NW
SE
(SF3)
75ms
1 km
(iii)
Survey extent
(iv)
25 Hz
36 Hz
31 Hz
(ii)
Sediment locally sourced from salt-high
(iii)
(i)
(SF3)
Inter-valley highs
(SF2)
(SF2)
Salt-collapse faults
Shelf-edge
Incised valleys diminish toward the shelf
2 km
(iv)

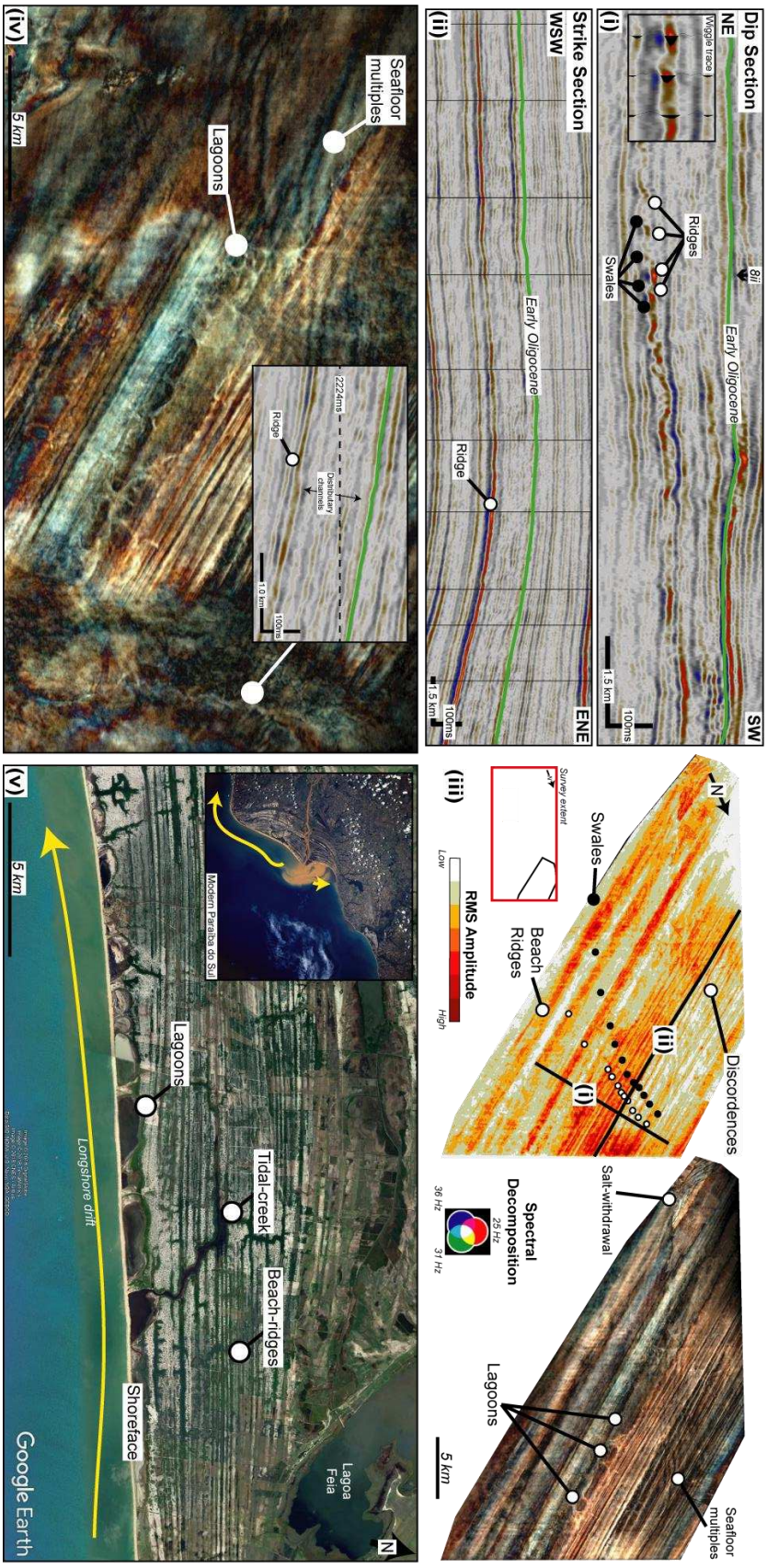
Dip Section
NE
SW
Wiggle Trace
Ridges
Swales
Early Oligocene
1.5 km
100ms
(i)
Strike Section
WSW
ENE
(ii)
Ridge
(iii)
N
Swales
Discordences
Beach Ridges
Survey extent
RMS Amplitude
Low
High
Salt-withdrawal
Spectral Decomposition
25 Hz
36 Hz
31 Hz
Seafloor multiples
Lagoons
5 km
(iv)
224ms
Distributary channels
Ridge
1.0 km
100ms
(v)
Modern Paraíba do Sul
Lagoons
Tidal-creek
Beach-ridges
Shoreface
Lagoa Feia
Longshore drift
Google Earth

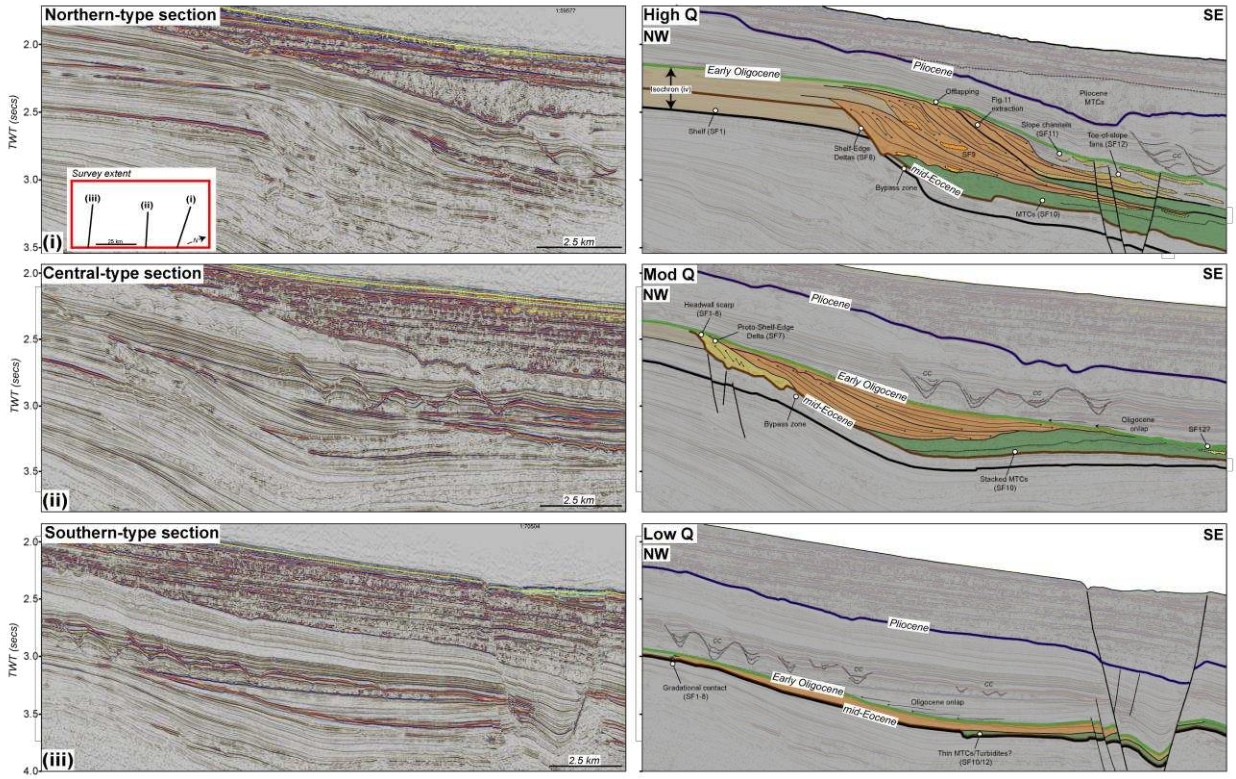
Northern-type section
Survey extent
(iii)
(ii)
(i)
(i)
2.5 km
TWT (secs)
2.0
2.5
3.0
3.5
High Q
NW
SE
Early Oligocene
Pliocene
Isochron (ii)
Offlapping
Fig 11 extraction
Pliocene MTCs
Shelf (SF1)
Slope channels (SF11)
Toe-of-slope fans (SF12)
Shelf-Edge Deltas (SF8)
SF9
Bypass zone
mid-Eocene
MTCs (SF10)
Central-type section
(ii)
2.5 km
Mod Q
Headwall scarp (SF1-6)
Proto-Shelf-Edge Delta (SF7)
Oligocene onlap
SF12?
Stacked MTCs (SF10)
Southern-type section
(iii)
2.5 km
4.0
Low Q
Gradational contact (SF1-8)
Thin MTCs/Turbidites? (SF10/12)

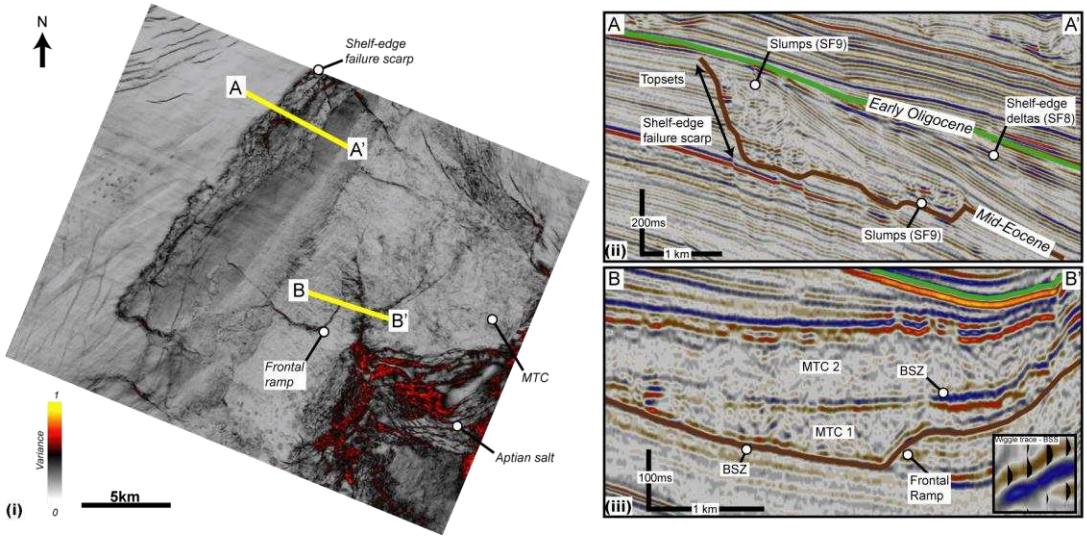
N
Shelf-edge failure scarp
A
A'
B
B'
Frontal ramp
MTC
Aptian salt
Variance
1
0
(i)
5km
A
A'
Slumps (SF9)
Topsets
Shelf-edge failure scarp
Early Oligocene
Shelf-edge deltas (SF8)
200ms
1 km
Slumps (SF9)
Mid-Eocene
(ii)
B
B'
MTC 2
BSZ
MTC 1
BSZ
100ms
1 km
Frontal Ramp
(iii)

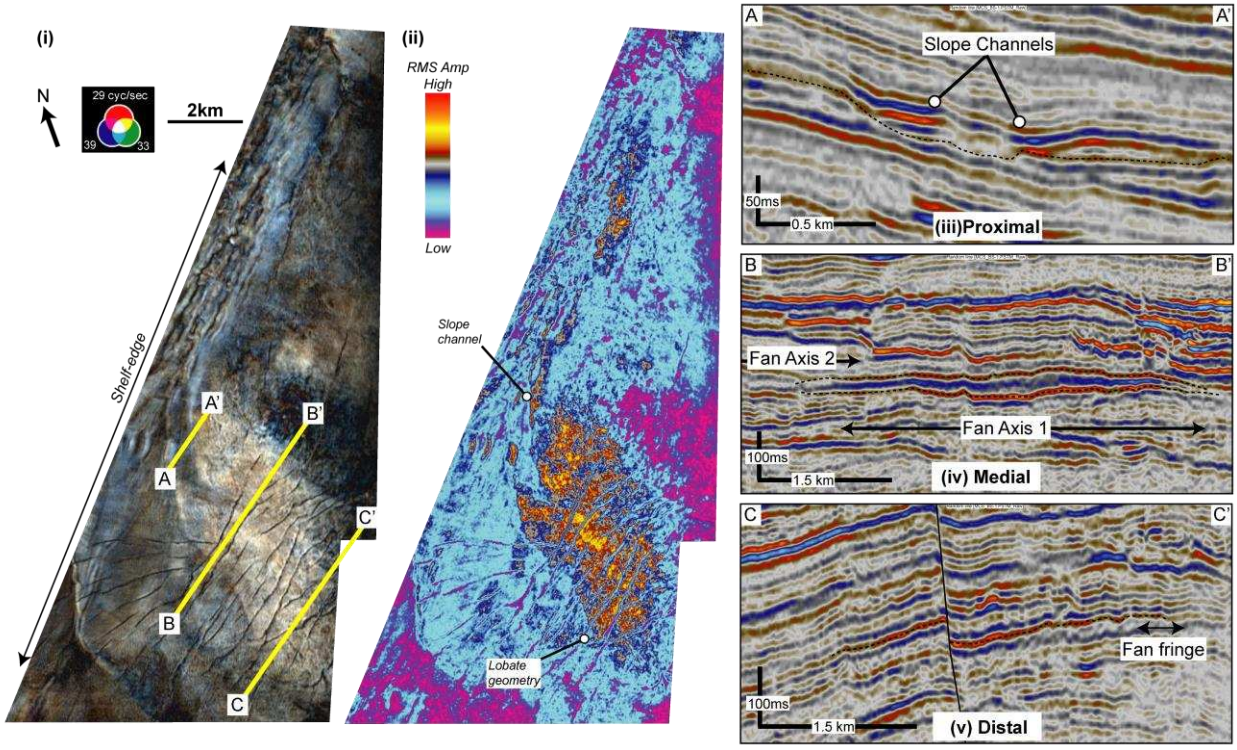
(i)
N
29 cyc/sec
39
33
2km
Shelf-edge
A
A'
B
B'
C
C'
(ii)
RMS Amp
High
Low
Slope channel
Lobate geometry
A
A'
Slope Channels
50ms
0.5 km
(iii)Proximal
B
B'
Fan Axis 2
Fan Axis 1
100ms
1.5 km
(iv) Medial
C
C'
Fan fringe
100ms
1.5 km
(v) Distal

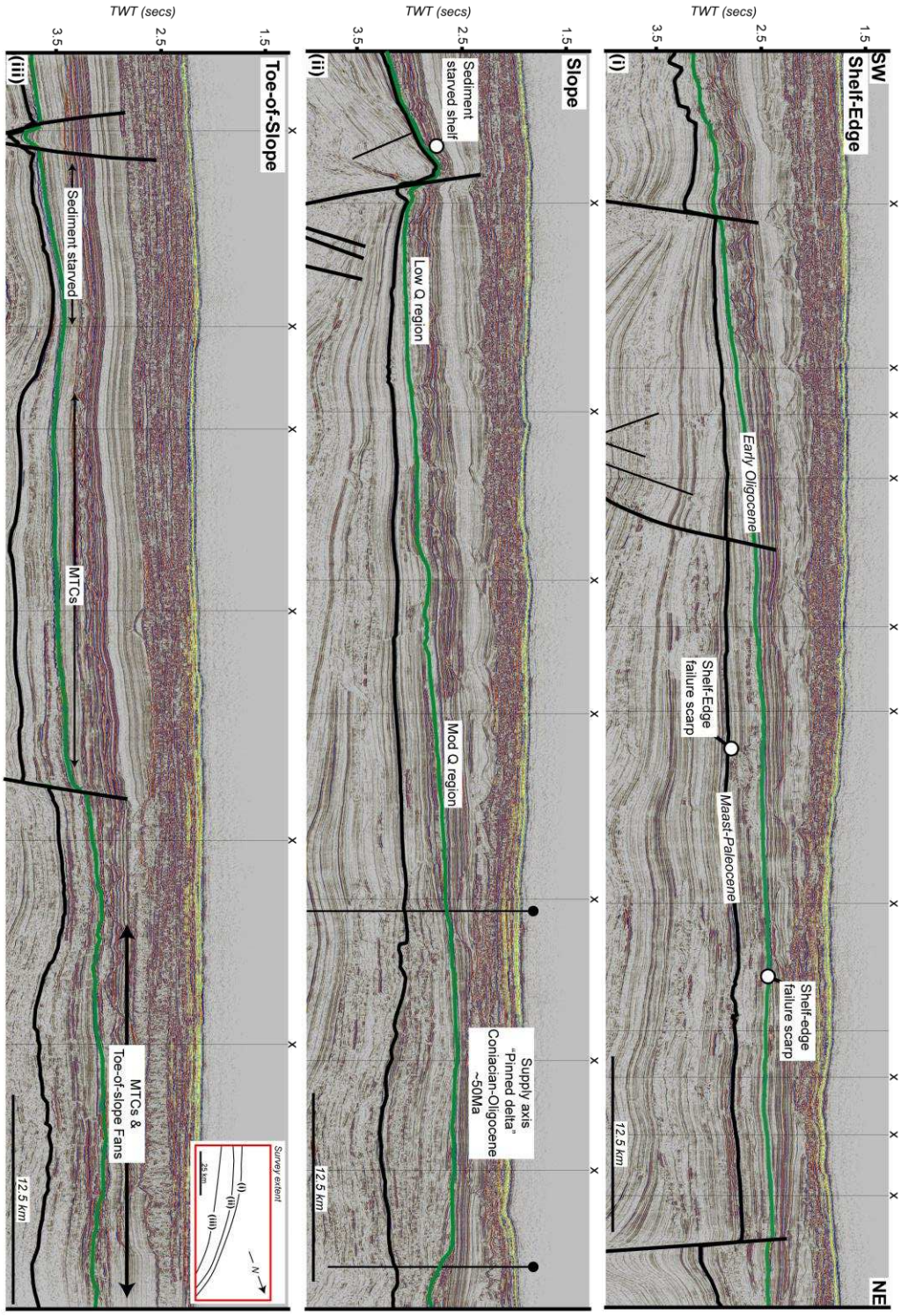
SW
NE
Shelf-Edge
Slope
Toe-of-Slope
TWT (secs)
(i)
(ii)
(iii)
Early Oligocene
Maast-Paleocene
Shelf-edge failure scarp
Shelf-Edge failure scarp
12.5 km
Supply axis "Pinned delta" Coniacian-Oligocene ~50Ma
Mod Q region
Low Q region
Sediment starved shelf
Sediment starved
MTCs
MTCs & Toe-of-slope Fans
Survey extent
N
25 km

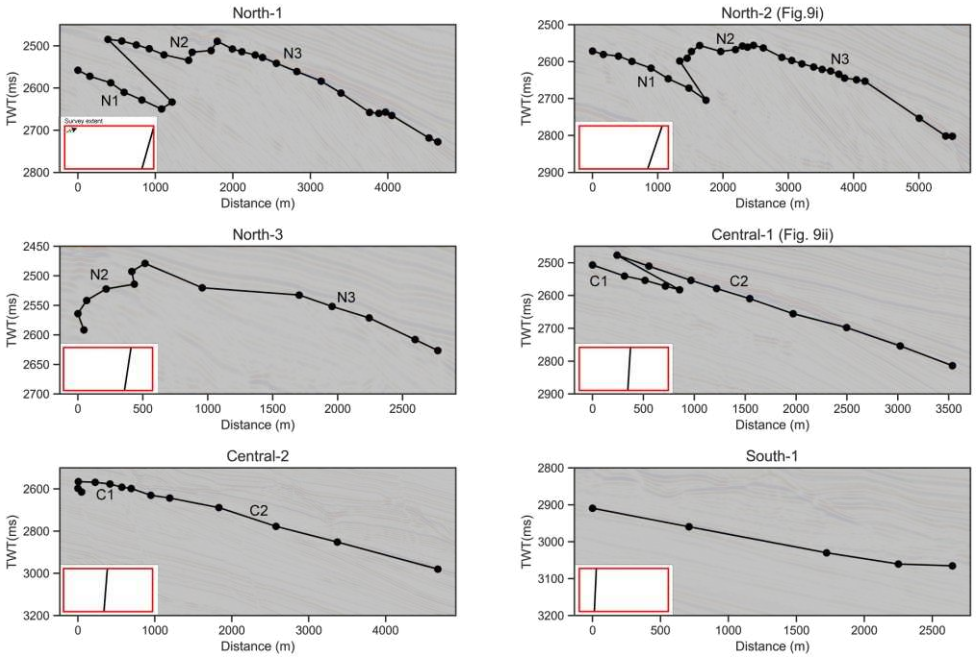
North-1
N1
N2
N3
Survey extent
TWT(ms)
Distance (m)
North-2 (Fig.9i)
N1
N2
N3
TWT(ms)
Distance (m)
North-3
N2
N3
TWT(ms)
Distance (m)
Central-1 (Fig. 9ii)
C1
C2
TWT(ms)
Distance (m)
Central-2
C1
C2
TWT(ms)
Distance (m)
South-1
TWT(ms)
Distance (m)

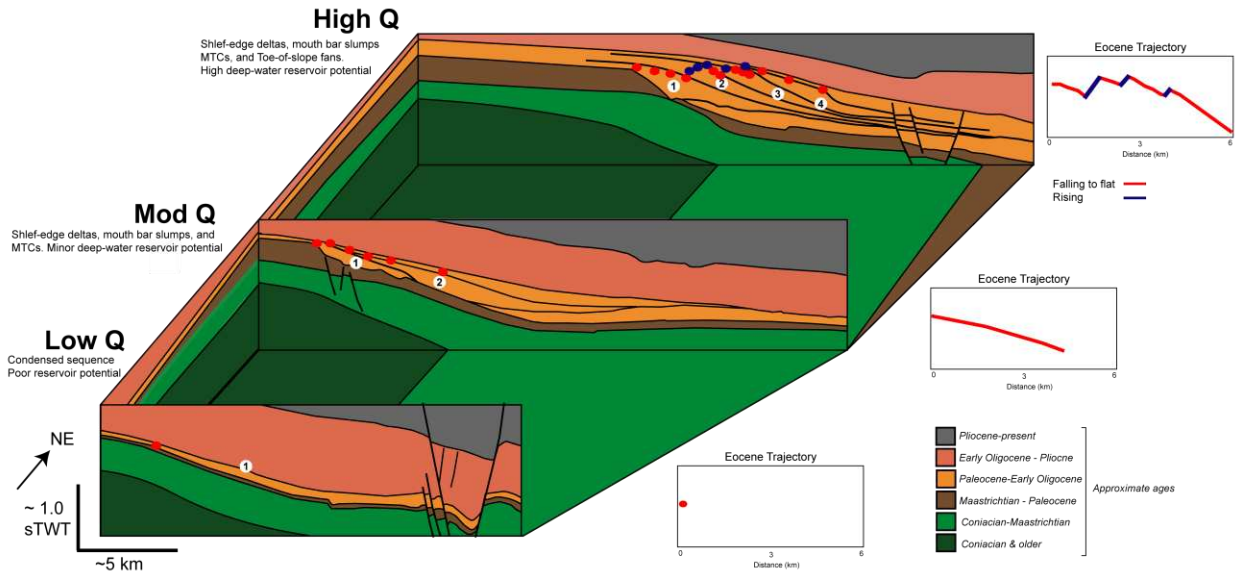
High Q
Shlef-edge deltas, mouth bar slumps
MTCs, and Toe-of-slope fans.
High deep-water reservoir potential
Mod Q
Shlef-edge deltas, mouth bar slumps, and
MTCs. Minor deep-water reservoir potential
Low Q
Condensed sequence
Poor reservoir potential
NE
~ 1.0
sTWT
~5 km
Eocene Trajectory
Distance (km)
Falling to flat
Rising
Eocene Trajectory
Distance (km)
Eocene Trajectory
Distance (km)
Pliocene-present
Early Oligocene - Pliocne
Paleocene-Early Oligocene
Maastrichtian - Paleocene
Coniacian-Maastrichtian
Coniacian & older
Approximate ages

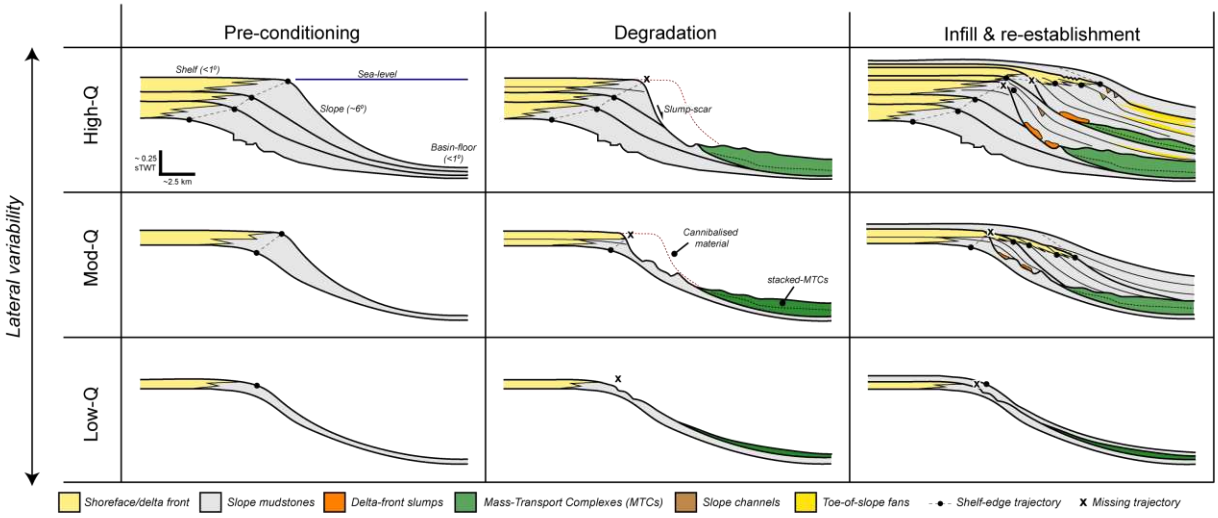
Pre-conditioning
Degradation
Infill & re-establishment
High-Q
Mod-Q
Low-Q
Lateral variability
Shelf (<1°)
Sea-level
Slope (~6°)
Basin-floor (<1°)
~ 0.25 sTWT
~2.5 km
Slump-scar
Cannibalised material
stacked-MTCs
Shoreface/delta front
Slope mudstones
Delta-front slumps
Mass-Transport Complexes (MTCs)
Slope channels
Toe-of-slope fans
Shelf-edge trajectory
Missing trajectory

Seismic Facies	Description	Geometry	Location (Fig.2 Index)	Example		Interpretation
SF1	Sub-parrallel, low-moderate amplitude, variable frequency and high continuity	Wedge W= >35km T= ~250ms L= >85km	Study wide Topset			**Shelf**
SF2	Low amplitude, low frequency and moderate continuity	Linear-Irregular W= 2-6.5km T= SR-100ms L= 14km	Northern Area Topset	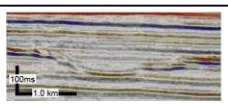	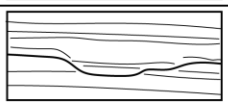	**Incised Valley Fill**
SF3	High amplitude, variable frequency, low continuity	Sinuous W= SR-1.35km T= SR-50ms L= 10km	Northern Area Topset	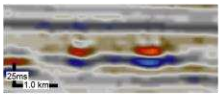	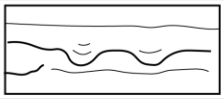	**Distributary Channels**
SF4	High-low amplitude, moderate frequency, high continuity	Thin linear-sets W= 0.1-1km T= 20ms L= 28km	Northern & Central Area Topset	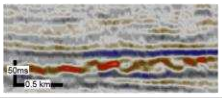	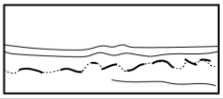	**Beach Ridges/ Strandplain**
SF5	High-low amplitude, moderate frequency, high continuity	Wide linear-sets W= 6km T= 75ms L= 28km	Northern & Central Area Topset	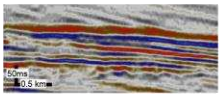	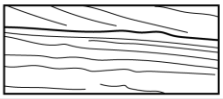	**Foreshore/ Upper Shoreface**
SF6	Low amplitude, low frequency, moderate continuity	Parallel-oblique clinoforms W= 7.8km T= SR-350ms L= 7.8km	Northern & Central Area Topset		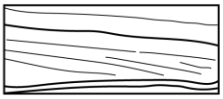	**Mid-Shelf Deltas**
SF7	Low amplitude, high-moderate frequency, low-moderate continuity	Oblique sigmoidal to sigmoidal clinoforms W= up to 5km T= 75-150ms L=<0.15->1.5km	Northern & Central Area Foreset	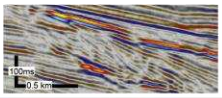	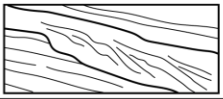	**Proto-Shelf -Edge Deltas**
SF8	High-low amplitude, high-moderate frequency, high-moderate continuity	Oblique sigmoidal to sigmoidal clinoforms W= up to 20km T= 200-500ms L= 6-10km	Study wide Foreset		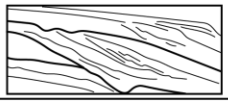	**Shelf-Edge Deltas**
SF9	High amplitude, high-moderate frequency, high-low continuity	Slope parallel elongate W= 75-200m T= 25-50ms L= 0.18-1.65km	Northern & Central Area Foreset	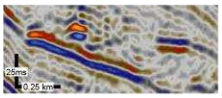	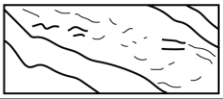	**Slumps**
SF10	High-low amplitude, moderate-low frequency, very low internal continuity, high bounding surfaces	Mounded W= up to 21km T= 75-600ms L= >27km	Study wide Bottomset	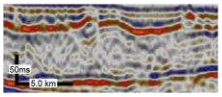	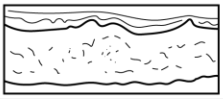	**Mass-Transport Complex (MTC)**
SF11	High amplitude, moderate-low frequency, moderate-low continuity	Sinuous W= SR-2km T=SR-40ms L=>10km	Northern Area Bottomset	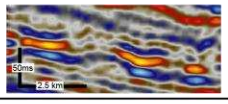	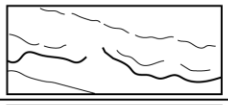	**Slope Channels**
SF12	High amplitude, moderate-low frequency, high-moderate continuity	Strike-elongate lobate W= up to 3.5km T= SR-65ms L= 8km	Northern Area Bottomset	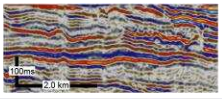	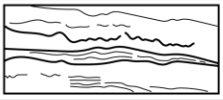	**Toe-of-slope Fans**

Facies	Morphometric Parameters				Examples
	Width (km)	Length (km)	Thickness (ms TWT)	Approx. Thickness (m) assuming vel = 2750 ms^{-1}	
SF1 (Shelf)	80+	35+	85-290	115-400	Figs. 4, 6, 9
SF2 (Incised Valley Fill)	2.00-6.5	14	VR-100	VR-140	Fig. 7
SF3 (Fluvial Channels)	0.05-1.35	11	VR-30	VR-40	Fig. 7
SF4 (Single Beach Ridges/Strandplain)	0.1-1.0	28+	20	28	Figs. 7, 8
SF5 (Foreshore/Upper Shoreface)	4-10	28+	40-75	55-105	Fig. 6
SF6 (Mid-Shelf Deltas)	7.8	4.25	175-350	240-480	Figs. 4, 5, 6
SF7 (Proto-Shelf-Edge Deltas)	5	2.75	75-150	105-205	Fig. 9
SF8 (Shelf-Edge Deltas)	20		200-500	275-685	Figs. 4, 9, 12
SF9 (Slumps)	0.18-1.65	0.075-0.2	25-50	35-70	Figs. 9, 10
SF10 (MTCs)	20	12+	75-275	105-375	Figs. 9, 10
SF11 (Slope Channels)	0.05-0.2	6+	VR-50	VR-70	Figs. 9, 11
SF12 (Toe-of-slope Fans)	3.5	6.75	VR-60	VR-83	Figs. 9, 11